博士論文

Electrochemical Properties of Metal-Hydride/Hydrogen-Gas Hybrid Electrode

金属水素化物/水素ハイブリッド電極の電気化学特性

上 里　裕 紀

広島大学大学院先端物質科学研究科

2019 年 3 月

目次

主論文

Abstract

Utilization of renewable energy is important to realize the CO_2 free and sustainable society without depending on fossil fuels in the world. High capacity, high efficiency and resource-rich energy storage technique is required for efficient utilization of renewable energy. Among them, many researchers are conducting study on secondary batteries and hydrogen-based energy storage systems. In this thesis, we study new technique combining the technology of nickel-metal-hydride (Ni-MH) battery and hydrogen.

We proposed "Hybrid Nickel-Metal Hydride/Hydrogen (Ni-MH/H_2) Battery" using high capacity AB_5-type metal hydride (MH) with high dissociation pressure (>0.1 MPa) and high-pressure hydrogen gas (H_2) as negative electrode active materials. The electrochemical properties are experimentally investigated, and the principle of this concept is discussed. The theoretically calculated electrochemical capacity of AB_5-type MH with high dissociation pressure were 380-400 $mAhg^{-1}$. These capacities were higher than the value of the AB_5-type MH in commercial battery (capacity: below 300 $mAhg^{-1}$, dissociation pressure: 0.012 MPa at 293 K). It was expected that the calculated gravimetric energy density of this hybrid battery increased up to 1.5 times of the commercial Ni-MH battery under 35 MPa of H_2 atmosphere. Additionally, it was also expected that the amount of used MH could be reduced to about 32wt.%.

The electrochemical properties of this battery under high-pressure H_2 atmosphere were investigated by the specially designed high-pressure electrochemical cell. It was clarified that H_2 gas can be utilized as an active material of negative electrode by the presence of the AB_5-type MH. It was confirmed that the electrochemical reaction at positive electrode was the same reaction as conventional Ni-MH batteries independent of the H_2 pressure in the cell. Additionally, it was also confirmed that the interface between MH and H_2 is key to utilize H_2, and the discharge capacity drastically decreased in a pressure atmosphere below the dissociation pressure of MH. These results suggested that a concept of this hybrid battery experimentally

demonstrated. The experimental cell voltages which were estimated from an averaged value of charge and discharge voltages at 50% of the capacities were consistent with the electro motive force estimated by dissociation pressures of AB_5-type MH. Additionally, the cell voltages were constant independently with internal pressure in the cell. These results indicated that the electrochemical potentials of this cell were determined by the thermodynamic parameters of MH, and electrochemical reactions proceed at the interface between MH and aqueous electrolyte solutions. Namely, AB5-type MH does not play the role as catalyst such as platinum (Pt) for fuel cells. This suggests that H2 is released after passing through the inside of MH as the atomic form during charge processes, and the H2 is dissociated into atoms and pass through MH during the discharging processes. Thus, it was expected that the gaseous H_2 was produced/consumed through the inside of the AB_5-type MH during charge/discharge reactions, and the gaseous H_2 reacted as absorbed hydrogen atom in the AB_5-type MH.

Contents

1 Introduction

1-1 Renewable energy

Renewable energy is natural energy without depletion, such as solar power, solar heat, hydropower, wind power, geothermal, ocean energy, and biomass. These renewable energy plays important roles to reduce the use of fossil fuel and greenhouse gas emissions. Therefore, various companies, institutes and universities are conducting research and development for utilization and storage of renewable energy to establish carbon dioxide (CO_2) free society.

1-1-1 Importance to utilization of renewable energy

The discovery of fossil fuels such as petroleum, coal and natural gas has drastically changed the social energy situation. The development of these utilization techniques had led to the industrial revolution that began around 1750. However, when these fossil fuels are used, various pollution gases such as CO_2 and nitrogen oxides (NO_x) are emitted in the atmosphere. Methane (CH_4) is also emitted during the production and utilization of fossil fuels. These gaseous by-products are called “greenhouse gas”.

One of the biggest environmental problems associated with using fossil fuels, is global warming. This problem is the rise in the average temperature of Earth’s atmosphere and oceans since the late 19th century, and it is considered that increase of greenhouse gases in the atmosphere is one of the factors. In fact, serious environmental problems such as unexpected/extreme weather and changes in ecosystems are found in recent years.

Nuclear power is CO_2 free energy using nuclear fuels such as uranium, and it was expected as next generation energy. However, it has many problems on safety, and serious damages due to the nuclear power plant accidents at Chernobyl and the Fukushima nuclear power plant accident in the eastern Japan great earthquake disaster are remembered.

Since the estimated reserve of fossil fuels and uranium is limited, its exhaustion is also a concern in the future. Therefore, for realizing a "sustainable society", it is necessary to select and utilize safe energy while dealing with exhaustion of energy resources and environmental problems.

Renewable energy is virtually free of resource exhaustion, and it can be safely converted into electric energy without emission of greenhouse gas or radioactive materials. Thus, it will be possible to realize a sustainable society by promoting to utilize renewable energy. However, renewable energy depends on natural conditions such as climate and geography. It also depends on sunlight hours and seasons. In other words, renewable energy is localized spatially and temporally. Renewable energy has to be converted to secondary energy such as electricity and hydrogen and be stored into media for responding the demand. Therefore, various energy storage technologies are required for efficient utilization of renewable energy in the world [1] [2].

1-1-2 Energy storage techniques for utilization of renewable energy

Energy storage technologies plays an important role to store and level renewable energy. These technologies can be classified into carrier and stationary storage, for leveling temporal and spatial variation.

Energy carrier

For the storage technique using energy carrier, energy is stored by using the chemical bonds of molecules via conversion processes, and it is controlled in a chemical reaction. After the release of chemical energy, the substance is often changed into entirely different substance. Recently, many researchers focus on energy carriers (liquid fuels) such as ammonia, methyl cyclohexane (C_7H_{14}), formic acid (HCOOH), and liquid hydrogen (H_2) are suitable as storage media of large amounts of energy for greater durations despite of low energy efficiency. These carriers are studied for utilization as a fuel of fuel cell directly or converted to hydrogen. Table 1-1 shows fundamental properties of energy carriers. Energy carriers have large energy densities above 1000 $Whkg^{-1}$ and 1000 WhL^{-1}.

Table 1-1-1 Fundamental properties of energy carriers

Properties	NH_3	C_7H_{14}	HCOOH	H_2 (liq.)
Molecular weight ($gmol^{-1}$)	17.03	98.19	46.03	2.016
Boiling point (°C)	-33	101	101	-253
Gravimetric energy density ($Whkg^{-1}$)	6260	1860	1540	39500
Volumetric energy density (WhL^{-1})	3760*[1]	1430	1880	2800*[2]
Energy for H_2 desorption ($kJmol\text{-}H_2^{-1}$)	30.6	67.5	31.5	0.899

*[1]1 MPa, 298 K, *[2]0.1 MPa, 20 K

Stationary energy storage

Stationary energy storage technologies are classified in the following groups: mechanical energy storage (MES), electrical energy storage (EES), thermal energy storage (TES), electrochemical energy storage (ECES).

MES techniques basically store energy as potential or kinetic energy. Kinetic energy storage includes flywheel energy storage (FES), besides potential energy storages includes pumped hydro storage (PHS), and compressed air energy storage (CAES). Although MES techniques are suitable for massive storage and has a longer life than other energy storage techniques, there are restrictions on locations and special operations techniques are necessary.

EES techniques are categorized into electrostatic energy storage such as conventional capacitors or supercapacitors (EDLC) and magnetic/current storage including superconducting magnetic energy storage (SMES). Although these techniques have relatively low energy density, there has high energy conversion efficiency and high response.

TES mainly uses materials that can be kept at either low or high temperatures in insulated containment to store energy in the form of heat. This technique is suitable for storage of solar heat and can be utilized for storing waste heat. However, this technique has a limitation of energy conversion efficiency according to Carnot's principle.

ECES such as hydrogen-based energy storage systems and secondary batteries, has been studied for local leveling of renewable energy because of their large energy density [3] [4] [5]. The hydrogen-based system is fuel cell system using H_2 gas. The secondary batteries are lithium-ion (Li-ion) batteries, nickel-metal hydride (Ni-MH)

batteries, nickel-cadmium (Ni-Cd) batteries, sodium-sulfur (NaS) batteries, redox-flow batteries, and lead-acid batteries.

Fig.1-1-1 shows Gravimetric and volumetric energy densities of physical energy storage. Secondary battery has high energy densities and high energy efficiency from 70-90%, where the efficiency is defined by output energy divided by input energy. Hydrogen-based energy storages converts electricity into H_2 via electrolyser. H_2 can be stored in hydrogen storage systems. Regenerative Fuel Cells (RFC) is utilized to reproduce electricity. H is a resource-rich element because it is generated by water electrolysis reaction. A typical hydrogen-based energy storage system consists of a water electrolyser, a hydrogen storage tank, and a fuel cell. This system can store large amount of electrical energy in the form of H_2 (35 MPa high-pressure H_2 tank 2300 $Whkg^{-1}$, 690WhL^{-1}), and then the energy efficiency is about 40%, which is half value of the secondary battery [6].

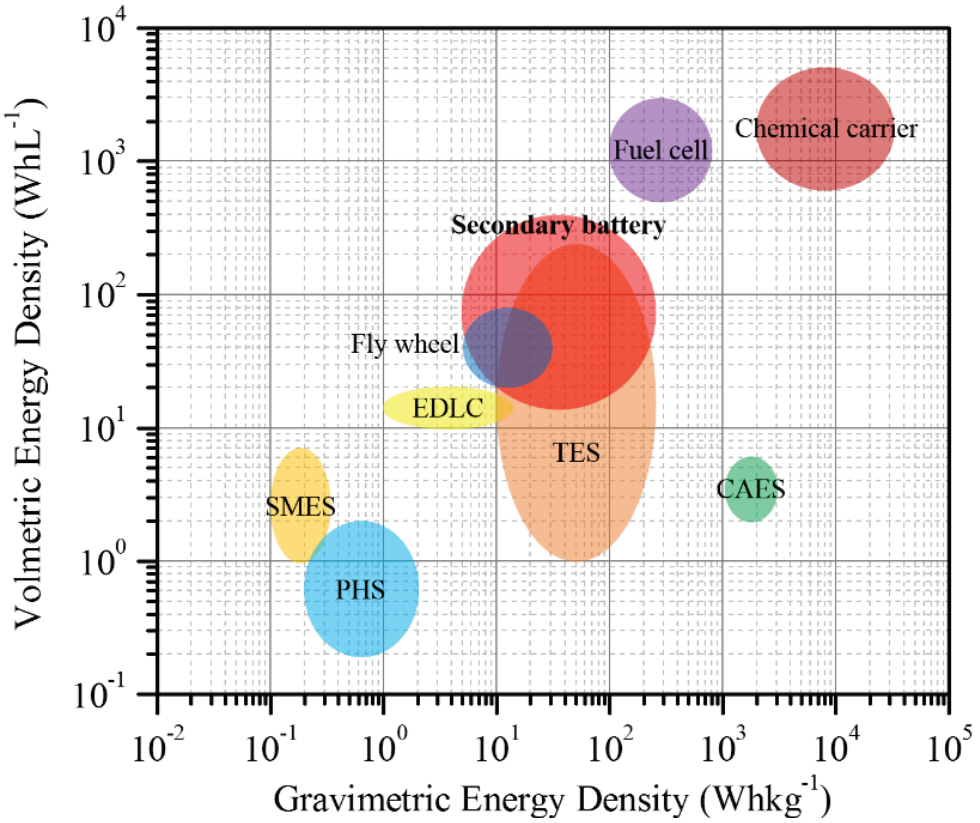

Fig. 1-1-1 Gravimetric and volumetric energy densities of energy storage techniques [7] [8] [9]

Fig. 1-1-2 shows volumetric and gravimetric energy densities of secondary batteries. The volumetric energy densities of Ni-MH, NaS, and Li-ion batteries have similar values, although the gravimetric energy density of Ni-MH batteries is smaller than the value of Li-ion and NaS batteries.

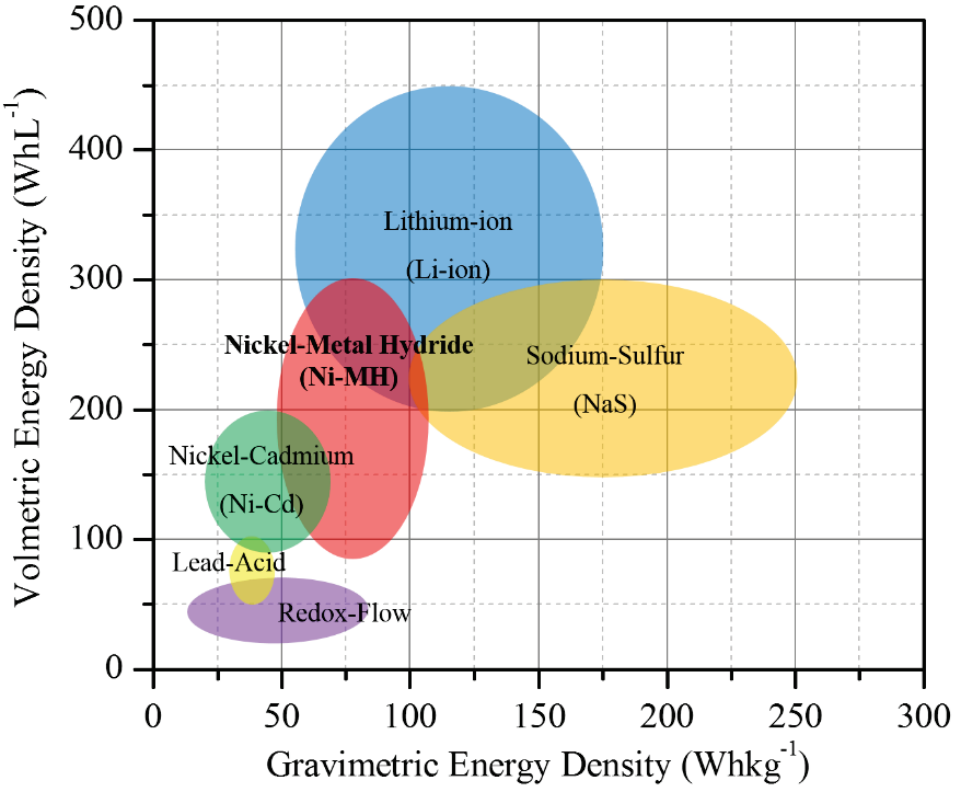

Fig. 1-1-2 Gravimetric energy densities and volumetric energy densities [7] [8]

1-2 Secondary batteries using hydrogen for stationary energy storage

As described above, hydrogen is a resource-rich element and generated by water electrolysis reaction. In our research, we focused on the secondary battery using the hydrogen because high energy efficiency can be expected.

1-2-1 Nickel-hydrogen battery

A nickel-hydrogen (Ni-H_2) battery is a secondary battery which has been researched and developed in NASA as a power source for an artificial satellite instead of a nickel-cadmium (Ni-Cd) battery.

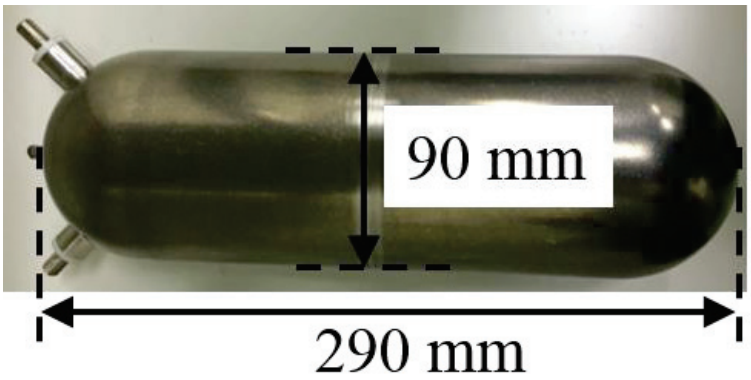

Fig. 1-2-1 Overview of Nickel-hydrogen battery

Fig. 1-2-1 shows overview of nickel-hydrogen battery in which hydrogen pressure is 6.6 MPa. The gravimetric and volumetric energy densities are 57.5 $Whkg^{-1}$, 101 WhL^{-1}, respectively. This battery has platinum (Pt) as a hydrogen dissociation catalyst on the negative electrode. Hydrogen gas (H_2) of about 8 MPa is used as the

negative electrode active material in the Ni-H_2 battery although conventional secondary batteries has solid electrode active materials, where cadmium (Cd) is used as the negative electrode active material in the Ni-Cd battery, As a feature, it is possible to manage the state of charge by the pressure of hydrogen gas, it has resistant to overcharge/overdischarge and has a long life enough to withstand charging and discharging more than 10,000 cycles. On the other hand, higher gas pressure is necessary to increase the density of H_2 for improving the capacity of battery. Although the Ni-H_2 battery has been studied and put to practical use for satellites requiring high maintenance stability and high operational stability, it has not been studied for utilization as a stationary energy storage.

1-2-2 Nickel-metal hydride battery

Nickel-metal hydride (Ni-MH) batteries are known as rechargeable small portable batteries and batteries in hybrid vehicles (HEV). Fig. 1-2-2 shows Overview of Ni-MH battery for hybrid vehicle.

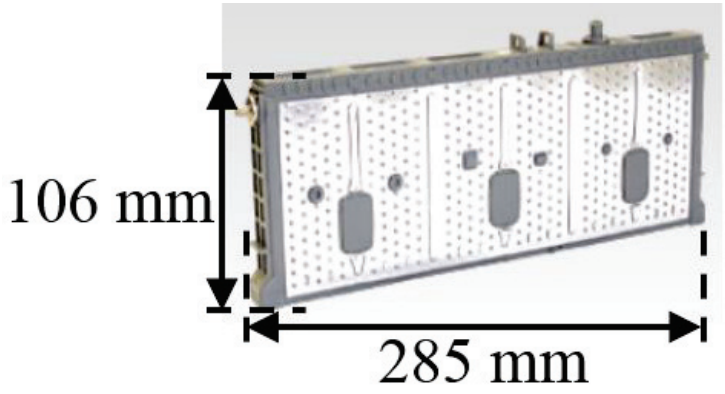

Fig. 1-2-2 Overview of Nickel-MH battery for hybrid vehicle.

As the negative electrode active material of this battery, hydrogen storage alloy is used instead of Cd of the Ni-Cd battery. After various hydrogen storage alloys were discovered since 1968, researchers have been studying them to use as a negative electrode active material. The hydrogen storage alloys are stable even in high concentration alkaline aqueous solution and electrochemically absorb/desorb hydrogen. Ni-MH battery was mass produced as practical application in Japan in 1990.

This battery has a good safety, cycle properties, and cost performance, compared with lithium-ion battery [10] [11]. The Ni-MH battery is also known as secondary battery using hydrogen for stationary energy storage [12] [13]. This battery stores electric energy as the solid hydride phase of alloys, and then energy efficiency of this battery is 70-90% [14].

Fig.1-2-3 shows schematic picture of conventional Ni-MH battery. At the positive electrode, the electrochemical charge/discharge reactions are expressed by the following equation:

$$\mathrm{Ni(OH)_2} \rightleftarrows \mathrm{NiOOH} + \mathrm{H_2O} + \mathrm{e^-} \tag{1-1}$$

where, facing right and left show charge and discharge steps, respectively. At the negative electrode, the reactions are expressed by the equation:

$$\mathrm{M} + \mathrm{H_2O} + \mathrm{e^-} \rightleftarrows \mathrm{MH} + \mathrm{OH^-} \tag{1-2}$$

where M and MH are a hydrogen storage alloy and its hydrogen absorbed state (metal hydride). Then, the total reactions are described as follows:

$$\mathrm{Ni(OH)_2} + \mathrm{M} \rightleftarrows \mathrm{NiOOH} + \mathrm{MH} \tag{1-3}$$

At both electrodes, oxidation/reduction reactions take place in an alkaline electrolyte such as 30 wt.% KOH aqueous solution.

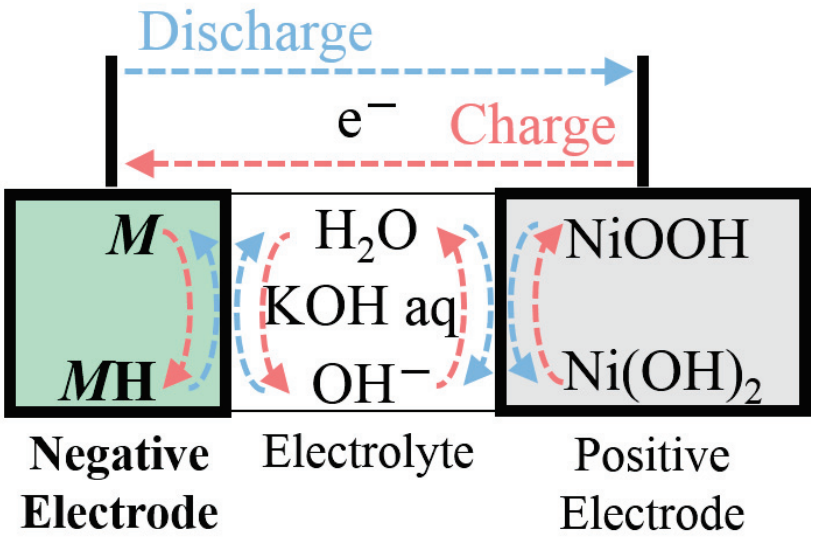

Fig. 1-2-3 Schematic diagram of Ni-MH battery.

The hydrogen storage alloy M is made of a metal A having high affinity with hydrogen such as magnesium (Mg), lanthanum (La), titanium (Ti), and B having low affinity with hydrogen such as nickel (Ni), manganese (Mn), iron (Fe), cobalt (Co). Hydrogen storage alloys having various compositions such as A_2B, AB, AB_2, and AB_5 have been studied for use as the negative electrode active materials. Among them, the AB_5-type hydrogen storage alloy has high stability, is easy to be activated, and has high cycle characteristics, thus AB_5-type alloys has been widespread as a practical negative electrode active material. Currently, the AB_5-type alloy with 290 mAh/g of gravimetric capacity (density 8.0 g/cm^3) is commercially used for negative electrode active materials

[15] [16] [17]. For these alloys used in commercial batteries, plateau dissociation pressure is 0.01 - 0.02 MPa at 293 K to prevent increasing inside pressure above 0.1 MPa at maximum working temperature of 333 K [16] [18] [19].

1-3 Hybrid Tank (High-pressure MH tank)

Hydrogen storage tank filled a hydrogen storage alloy below hydrogen gas pressure of 1 MPa (MH tank) was developed for fuel cell vehicles [20]. After that, high pressure gas technology has been advanced in the field of hydrogen [21] [22]. It has been reported that "Hybrid Hydrogen Tank (High-pressure MH Tank)" using hydrogen storage alloys with high dissociation pressure and high-pressure hydrogen gas at 35 MPa can improve hydrogen storage performances such as storage capacity and low temperature performance of the MH tank [23] [24]. Fig. 1-3-1 shows schematic diagram of Hybrid Hydrogen Tank (High-pressure MH Tank), and the hydrogen densities of the hybrid hydrogen tank are 1.4 times of the conventional MH tank [23].

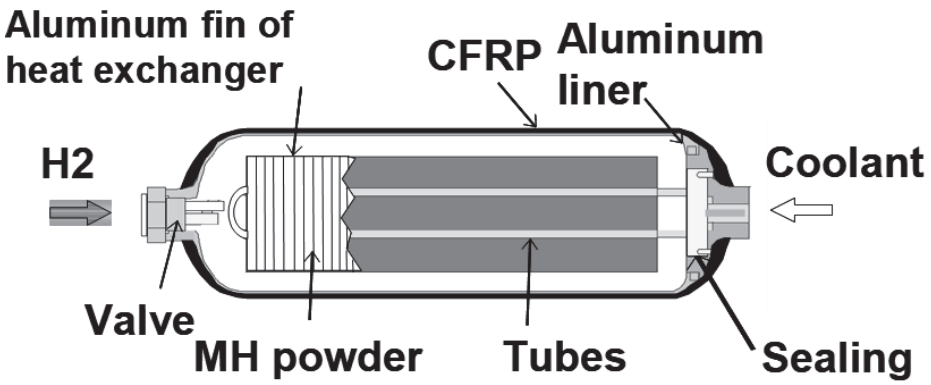

Fig.1-3-1 Schematic diagram of Hybrid Hydrogen Tank (High-pressure MH Tank) [23]

1-4 Thermodynamic and electrochemistry of metal hydride

Thermodynamics on the solid-gas phase reaction of metal hydride

The thermodynamics of the hydrogen-metal systems can be understood through the phase diagram. The phase diagram of the metal-hydrogen system can be expressed as a function of temperature and pressure of the surrounding H_2 gas. Thus, the equilibrium metal-hydrogen phase diagram is constructed from the Pressure-Concentration-Isothermal (PCI) curves as shown in Fig. 1-4-1 (a), which is obtained by isothermal measurements at several temperatures.

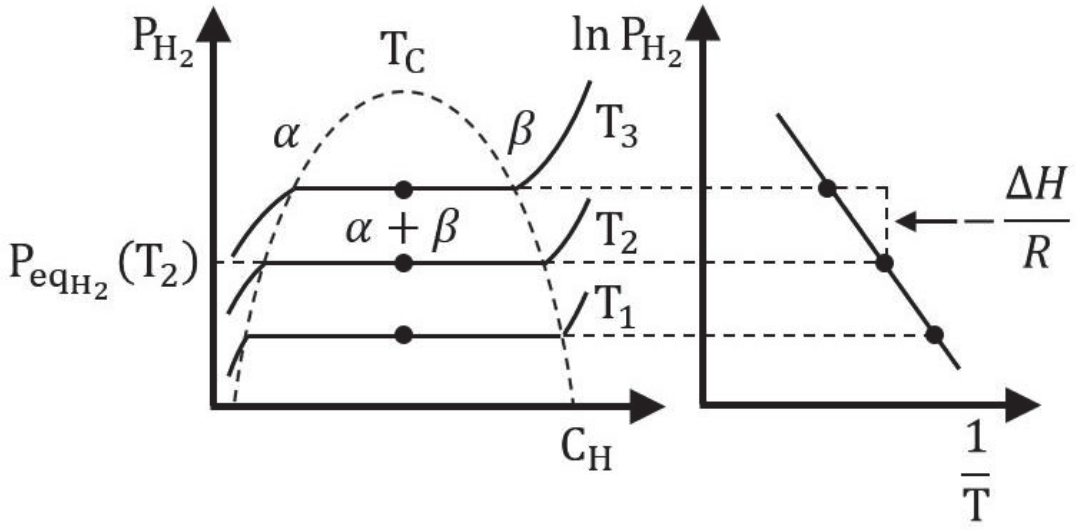

Fig. 1-4-1. (a) PCI diagram and (b) van't Hoff plot [25].

In the first stage of hydrogenation which is low hydrogen concentration region shown as left-side slope in PCI curve (Fig 1-4-1 (a)). Hydrogen starts to dissolve in metal lattice with increasing hydrogen pressure, indicating appearance of the solid solution which is denoted as the α-phase. The crystal structure of the α-phase is basically the same

as that of the host metal, and its cell volume is expanded by forming solid solution. In this region, hydrogen is successively absorbed in metal with increasing hydrogen pressure. The relation between hydrogen gas pressure and hydrogen concentration in this region is described by Sievert's law in the following equation,

$$\sqrt{P} = \mathrm{K}_s x \tag{1-4}$$

where P is hydrogen pressure, Ks Sievert's constant, x hydrogen concentration. This equation shows that the hydrogen concentration increases in proportion to the square root of hydrogen pressure in the low concentration region. In the second stage which is the horizontal region on the PCI curves in Fig. 1-4-1 (a), a hydride, which is denoted as β-phase, is formed by the occupation of hydrogen in the interstitial sites and changing from the α-phase. When the β-phase is formed, the crystal structure of the host metal is generally changed by forming the bond between hydrogen and metal atoms. In this region, two phases of α- and β- coexists and hydrogen pressure has to be constant although the hydrogen concentration is continuously increased by growing of the β-phase. This phenomenon is described by the Gibbs phase rule in the following equation,

$$\mathrm{f} = \mathrm{c} - \mathrm{p} + 2 \tag{1-5}$$

where f is the degrees of freedom, c and p are the number of components and phases in the system, respectively. In the case of $f = 1$, only one parameter among temperature, hydrogen pressure, or concentration can be chosen and other parameters are uniquely determined. Therefore, the hydrogen pressure as a function of hydrogen concentration in

the isothermal condition is kept at constant pressure in the PCI measurement. This constant pressure is generally called equilibrium (or plateau-) pressure P_{eq}. In the case of $f \neq 1$, no constant pressure region is appeared such as the low concentration region ($f = 2$) in Fig. 1-4-1 (a). Moreover, all parameters are uniquely determined in the case of $f = 0$. When operation temperature is raised up, the plateau region is disappeared through the critical point T_c, above which the α-phase continuously transforms to the β-phase with increasing hydrogen concentration.

In the final stage which is the region after the plateau area, pressure is further raised, and hydrogen concentration continues to increase until the limit. Absorbed hydrogen in this stage is dissolved to the hydrogen holes in the β-phase.

The slope and the width of the equilibrium plateau region are important for hydrogen storage applications. A flat plateau enables the reversible absorption and desorption of hydrogen in a metal and from a metal hydride, respectively, by controlling hydrogen pressure around P_{eq}. The width of the plateau region reveals the available amount of hydrogen. The hydrogen storage capacity depends on the relative thermodynamic stability of hydrogen in the host metal. The hydrogen absorption reaction to form the solid solution or a metal hydride phase is either exothermic or endothermic process, which can be understood by the enthalpy change ΔH. Here, ΔH is defined as a difference in relative stability between dehydrogenated and hydrogenated phases. This value can be directly estimated from the PCI curves which is obtained by measuring equilibrium pressure at several temperatures as shown in Fig. 1-4-1 (b).

The thermodynamics for the formation of solid solution between hydrogen and metal can be described in the following way;

The reaction of metal (M) with gaseous hydrogen in the molar ratio of $x/2$ is expressed in

the following reaction equation,

$$\mathrm{M(s)} + \frac{x}{2}\mathrm{H_2(g)} \rightleftarrows \mathrm{MH}_x\mathrm{(s)} \tag{1-6}$$

Under equilibrium condition, the chemical potential of the molecular hydrogen gas, μ_g, is equal to the chemical potential of the hydrogen atoms in solid solution μ_α.

$$\frac{1}{2}\mu_\mathrm{g}(T,p) = \mu_\mathrm{a}(T,p,x) \tag{1-7}$$

Gaseous hydrogen can be considered as an ideal gas at relatively low pressures. Therefore, the chemical potential of gaseous hydrogen can be described by calculating the partition functions Z_t, Z_r and Z_v for translational, rotational and vibrational motions, respectively, of ideal diatomic molecules, which is based on statistical thermodynamics as follows,

$$\begin{aligned}\mu_\mathrm{g}(T,p) &= kT\ln(Z_t \cdot Z_r \cdot Z_v) - E_\mathrm{d} \\ &= \mathrm{k}T\ln\frac{p_{\mathrm{H_2}}}{p_0} - E_\mathrm{d}\end{aligned} \tag{1-8}$$

$$p_0(T) = \frac{16(\pi k)^{\frac{7}{2}} M_0^{\frac{5}{2}} {r_0}^2}{h^5} T^{\frac{7}{2}} \tag{1-9}$$

where k is the Bolzman constant, E_d is the dissociation energy of a hydrogen molecule, M_0 is the mass of a hydrogen atom, r_0 is the distance between the hydrogen atoms, h is the Plank's constant, and $p_0(T)$ is the standard pressure which is generally defined as 1.03×10^5 Pa (~0.1 MPa) at 7.7 K [26].

The chemical potential of the hydrogen atoms in metal is defined by the Gibbs free energy, which is expressed by enthalpy H_α and entropy S_α of the solid solution,

$$\mathrm{G}(T,p) = H_a - TS_a \tag{1-10}$$

where $S\alpha$ is composed of excess entropy of solution $S\alpha e$ and ideal configurational entropy of hydrogen atom in metal $S\alpha i$,

$$S_a = S_{ae} + S_{ai} \tag{1-11}$$

$$S_{ai} = -k \ln\left\{\frac{r!}{x!(r-x)!}\right\} \tag{1-12}$$

where r and x are the number of interstitial sites and hydrogen occupying these sites (per metal atom), respectively. By using Strling's approximation,

$$\ln(N!) = N \ln N - N \tag{1-13}$$

$S_{\alpha i}$ is approximated by,

$$S_{ai} = kr \ln\left\{\frac{r}{r-x}\right\} - kx \ln\left\{\frac{x}{r-x}\right\} \tag{1-14}$$

Therefore, the chemical potential of hydrogen atom in the solid solution is described as follows, assuming that the partial enthalpy and entropy of the non-configurational part of hydrogen in the solid solution are given by h_α and $s_{\alpha e}$, respectively,

$$\mu_{\mathrm{a}}(T,p,x) = \frac{\partial G}{\partial x} = h_a - T_{S_{ae}} + kT\ln\left\{\frac{x}{r-x}\right\} \tag{1-15}$$

$$H_a = xh_a, \qquad S_{ae} = xs_{ae}$$

In the case of low hydrogen concentrations with $x << r$, the following approximation is derived,

$$\ln\left\{\frac{x}{r-x}\right\} \rightarrow \ln x - \ln r \tag{1-16}$$

and then following equation is obtained,

$$\mu_{\mathrm{a}}(T,p,x) = \frac{\partial G}{\partial x} = h_a - T_{S_{ae}} + k\ln x - kT\ln r \tag{1-17}$$

Taking into account that the chemical potential of hydrogen gas is equal to that of hydrogen in the solid solution, Eq. (1-4) becomes

$$\mathrm{k}T\ln\left\{\frac{p_{\mathrm{H_2}}}{p^0(T)}\right\}^{\frac{1}{2}} - \frac{1}{2}E_{\mathrm{d}} = h_a - T_{S_{ae}} + kT\ln\left\{\frac{x}{r-x}\right\} \tag{1-18}$$

Finally, the following equation is obtained in the case of low hydrogen concentration in the solid solution,

$$x = K_s\ln\left\{\frac{p_{\mathrm{H_2}}}{p^0(T)}\right\}^{\frac{1}{2}} \tag{1-19}$$

where

$$K_{\mathrm{s}}(T) = \exp\left(\frac{{}^{T}S_{ae} - h_a - \frac{1}{2}E_{\mathrm{d}} + kT\ln r}{kT}\right) \tag{1-20}$$

This is called Sievelt's law.

In the plateau region below critical temperature T_{c}, thermodynamics of hydride formation is described in the following way;

Here, the following hydrogen absorption reaction between a material A and hydrogen is considered.

$$a\mathrm{A} + b\mathrm{H_2} \rightarrow a\mathrm{AH}_{2b} \tag{1-22}$$

The Gibbs's free energy ΔG of this reaction can be expressed by using enthalpy change ΔH, entropy change ΔS and temperature T in the following equations,

$$\begin{aligned}\Delta G &= \Delta H - T\Delta S \\ &= aH_{\mathrm{AH}} - aH_{\mathrm{A}} - bH_{\mathrm{H_2}} - T\left(aS_{\mathrm{AH}} - aS_{\mathrm{A}} - bS_{\mathrm{H_2}}\right)\end{aligned} \tag{1-23}$$

where H_{AH}, $H_{A,}$ and H_{H2} are the enthalpy of $A\mathrm{H}_{2b}$, A, and H_2, respectively. S_{AH}, S_A, and S_{H2} are the entropy of $A\mathrm{H}_{2b}$, A, and H_2. The standard entropy of gas phase can be separated to standard entropy $S_{0\ H2}$, which is the entropy of hydrogen molecule at 0.1 MPa, and the entropy change of hydrogen gas due to the reaction as given by the following equation,

$$S_{\mathrm{H_2}} = S^0{}_{\mathrm{H_2}} - \mathrm{R}\ln\left\{\frac{p_{\mathrm{eq}_{\mathrm{H_2}}}}{p^0(T)}\right\} \quad (1\text{-}24)$$

where R is the gas constant and p_{eq} is the equilibrium pressure. Considering Eqs. (1-21), (1-22), and (1-23), following equation is defined,

$$\Delta S^0 = aS_{\mathrm{AH}} - aS_{\mathrm{A}} - bS^0{}_{\mathrm{H_2}} \quad (1\text{-}24)$$

Generally, the standard enthalpy of simple substance should be zero. In the case of thermochemical equilibrium condition, ΔG is zero. And then, the following equation is obtained,

$$\ln\left\{\frac{p_{\mathrm{eq}_{\mathrm{H_2}}}}{p^0(T)}\right\} = \frac{\Delta H^0}{\mathrm{R}T} - \frac{\Delta S^0}{\mathrm{R}} \quad (1\text{-}25)$$

This equation is called the van't Hoff equation. The ΔH and ΔS values can be experimentally estimated. The slope and the intercept in the plot of $\ln(p_{eq}/p_0(T))$ versus $1/T$ give ΔH and ΔS values, respectively, as shown in Fig. 1-1 (b). This plot is called the van't Hoff plot. Various enthalpy and entropy changes of the hydrogenation reaction of metals are shown in Table 1-2 [27]. For mobile storage, target thermodynamic properties is p_{eq} = 1~10 bar at 0~100 °C corresponding to ΔH = 15~24 kJ/mol H_2 for conventional hydrogen storage alloys (MH) [28].

Electrochemistry on the solid-liquid phase reaction of metal hydride

In the electrochemical hydrogen absorption / desorption reactions of the hydrogen storage alloy, reaction equation (1-2) can be assumed as follows,

Surface on the alloy: $2H_2O + e^- \rightleftarrows 2H + 2OH^-$ (1-26)

Hydrogenation of the alloy： $M + H_2 \rightleftarrows MH_2$ (1-27)

Overall reaction： $M + 2H_2O + e^- \rightleftarrows MH_2 + 2OH^-$ (1-28)

Here, H is hydrogen which is solved in the hydrogen storage alloy or its hydride. When the hydrogen storage alloy changes the amount of hydrogen inside the alloy by charging and discharging, the reaction equilibrium such as the formula (1-26) is established between the hydrogen dissolved in the alloy and the water of the electrolytic solution through the alloy surface. Additionally, in two-phase coexisting regions of the hydrogen solid solution phase and the hydride phase, reaction equilibrium is established such as the formula (1-27) between hydrogen solved in the alloy and hydride of the alloy. Because hydrogen is absorbed/desorbed through the alloy surface, the electrochemical reaction equilibrium potential of the negative electrode is determined by the reaction of the formula (1-26). This potential E_{eq} (H_2O/H) is given by Nernst's equation as follows.

$$E_{\mathrm{eq}}(\mathrm{H_2O/H}) = E^0(\mathrm{H_2O/H}) + \frac{\mathrm{R}T}{\mathrm{F}} \ln\left\{\frac{a(\mathrm{H_2O})}{a(\mathrm{H})\cdot a(\mathrm{OH^-})}\right\} \quad (1\text{-}29)$$

where E^0 is standard electrode potential of equation (1-26), and this value is －0.828 V

vs SHE (Standard Hydrogen Electrode: +0.000 V), R is gas constant (8.314 J $K^{-1}mol^{-1}$), *T* is temperature (K), F is Faraday constant (96485 $Cmol^{-1}$).

In the electrochemical reaction system of this formula, water and hydroxide ions are present in a large amount relative to the solid solution hydrogen H, and the mole fraction can be regarded as 1. Therefore, each activities *a* (H) and *a* (OH^-) can be regarded as 1, and the equation (1-29) Can be expressed as follows.

$$E_{\mathrm{eq}}(\mathrm{H_2O/H}) = -0.828 - \frac{\mathrm{R}T}{\mathrm{F}}\ln\{a(\mathrm{H})\} \qquad (1\text{-}30)$$

On the other hand, the activity *a* (H) of solid solution hydrogen changes according to the reaction process. Since the initial and final stages of charging and discharging are a hydrogen solid solution phase of the alloy or a single phase of the hydride phase, the activity *a* (H) changes in accordance with the change in the hydrogen storage capacity. The reaction equilibrium as shown in the reaction formula (1-27) is established in the hydrogen solid solution phase of the alloy and the two-phase coexistence region of the hydride phase, and the activity *a* (H) has a constant value. Therefore, the reaction equilibrium potential of the negative electrode is determined according to the value of such activity *a* (H). The potential E_{eq} (H_2O/H) is synonymous with the reaction equilibrium potential E_{MH} of the hydrogen storage alloy negative electrode. Here, the log term including the activity *a* (H) corresponds to the thermodynamic parameter in the reaction with the hydrogen gas of the hydrogen storage alloy, and its reaction equilibrium constant and the activity *a* (H) are synonymous. Thus,

it can be written as follows.

$$\ln\{a(\mathrm{H})\} = \frac{1}{2}\ln\left\{\frac{p_{\mathrm{eq}_{\mathrm{H_2}}}}{\mathrm{p}^0(T)}\right\} \quad (1\text{-}31)$$

where $P_{\mathrm{eq}_{\mathrm{H_2}}}$ is the equilibrium pressure of hydrogen storage alloy (MPa), P^0 is standard pressure (0.101 MPa). From equations (1-30) and (1-31) above, the redox potential E_{MH} of the negative electrode is expressed by the following equation.

$$E_{\mathrm{MH}} = -0.828 - \frac{\mathrm{R}T}{2\mathrm{F}}\ln\left\{\frac{p_{\mathrm{eq}_{\mathrm{H_2}}}}{\mathrm{p}^0(T)}\right\} \quad (1\text{-}32)$$

It is understood that the redox potential of the hydrogen storage alloy negative electrode varies depending on the hydrogen association/dissociation equilibrium pressure of the alloy, from this equation.

Positive electrode reaction is expressed by the following equation.

$$\mathrm{Ni(OH)_2} \rightleftarrows \mathrm{NiOOH} + \mathrm{H_2O} + \mathrm{e^-} \quad (1\text{-}33)$$

Then the redox potential (standard electrode potential) of positive electrode is +0.52V Therefore, the electromotive force (open circuit voltage) in the charge/discharge reaction is

$$E_{\mathrm{EMF}} = 1.35 + \frac{\mathrm{R}T}{2\mathrm{F}}\ln\left\{\frac{p_{\mathrm{eq}_{\mathrm{H_2}}}}{\mathrm{p}^0(T)}\right\} \quad (1\text{-}34)$$

This equation indicates that electromotive force is proportional to logarithm of

dissociation pressure of hydrogen storage alloys.

Fig.1-4-2 shows Conceptive picture of battery circuit. In discharge state, operating voltage E_1 is low compared with electromotive force (open circuit voltage) E_{EMF}. E_1 is expressed by

$$E_1 = E_{\mathrm{EMF}} - I\mathrm{R} \tag{1-35}$$

where, I: current value, R: internal resistance composed of reaction resistance and diffusion resistance etc. Average discharge voltage (discharge voltage at 50% of the capacity) E_{d} is assumed to be proportional to E_1.

$$E_{\mathrm{d}} = \mathrm{A}E_1 \tag{1-36}$$

In charge state, operating voltage E_2 is high compared with E_0. E_2 is expressed by

$$E_2 = E_{\mathrm{EMF}} + I\mathrm{R} \tag{1-37}$$

Average charge voltage (charge voltage at 50% of the capacity) E_{c} is assumed to be proportional to E_2.

$$E_{\mathrm{c}} = \mathrm{A}E_2 \tag{1-38}$$

Substituting equations (1-35) and (1-36) into equations (1-37) and (1-38), respectively

$$\frac{E_{\mathrm{d}}+E_{\mathrm{c}}}{2} = AE_{\mathrm{EMF}} \tag{1-39}$$

Where $\frac{E_{\mathrm{d}}+E_{\mathrm{c}}}{2}$ is cell voltage. Cell voltage is defined by averaged value of charge and discharge voltage at 50% of the capacities.

Substituting equation (1-39) into equation (1-34)

$$\frac{E_{\mathrm{d}}+E_{\mathrm{c}}}{2} = \propto \ln\left\{\frac{p_{\mathrm{eq}_{\mathrm{H_2}}}}{\mathrm{p}^0(T)}\right\} \tag{1-40}$$

Equation (1-40) indicates that cell voltage linearly increase with the logarithm of the dissociation pressure.

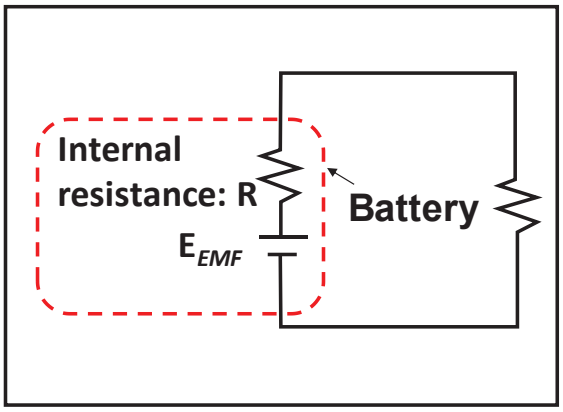

Fig. 1-4-2 Conceptive picture of battery circuit

Reference

[1] M.S. Guney, Y. Tepe, Renewable and Sustainable Energy Reviews, 75 (2017) 1187-1197.

[2] S.O. Amrouche, D. Rekioua, T. Rekioua, S. Bacha, International Journal of Hydrogen Energy, 41 (2016) 20914-20927.

[3] A. Eftekhari, B. Fang, International Journal of Hydrogen Energy, 42 (2017) 25143-25165.

[4] B. Dunn, H. Kamath, J.-M. Tarascon, Science, 334 (2011) 928.

[5] G. Gahleitner, International Journal of Hydrogen Energy, 38 (2013) 2039-2061.

[6] T. Bocklisch, Energy Procedia, 73 (2015) 103-111.

[7] J.M. Tarascon, M. Armand, Nature, 414 (2001) 359.

[8] X. Luo, J. Wang, M. Dooner, J. Clarke, Applied Energy, 137 (2015) 511-536.

[9] I. Sarbu, C. Sebarchievici, Sustainability, 10 (2018).

[10] B. Pierozynski, International Journal of Electrochemical Science, 6 (2011) 860-866.

[11] J. Kleperis, G. Wójcik, A. Czerwinski, J. Skowronski, M. Kopczyk, M. Beltowska-Brzezinska, Journal of Solid State Electrochemistry, 5 (2001) 229-249.

[12] D. Linden, T.B. Reddy, Handbook of Batteries. 3rd, 2002.

[13] K. Nishimura, T. Takasaki, T. Sakai, Journal of Alloys and Compounds, 580 (2013) 353-358.

[14] W.H. Zhu, Y. Zhu, Z. Davis, B.J. Tatarchuk, Applied Energy, 106 (2013) 307-313.

[15] A. Taniguchi, N. Fujioka, M. Ikoma, A. Ohta, Journal of Power Sources, 100 (2001) 117-124.

[16] K. Suzuki, N. Yanagihara, H. Kawano, A. Ohta, Journal of Alloys and Compounds,

192 (1993) 173-175.

[17] T.K. Ying, X.P. Gao, W.K. Hu, F. Wu, D. Noréus, International Journal of Hydrogen Energy, 31 (2006) 525-530.

[18] T. Sakai, Materia Japan, 36 (1997) 99-103.

[19] F. Feng, M. Geng, D.O. Northwood, International Journal of Hydrogen Energy, 26 (2001) 725-734.

[20] M.V. Lototskyy, I. Tolj, L. Pickering, C. Sita, F. Barbir, V. Yartys, Progress in Natural Science: Materials International, 27 (2017) 3-20.

[21] D. Mori, K. Hirose, International Journal of Hydrogen Energy, 34 (2009) 4569-4574.

[22] J. Zheng, X. Liu, P. Xu, P. Liu, Y. Zhao, J. Yang, International Journal of Hydrogen Energy, 37 (2012) 1048-1057.

[23] D. Mori, N. Kobayashi, T. Matsunaga, K. Toh, Y. Kojima, Materia Japan, 44 (2005) 257-259.

[24] Y. Kojima, Y. Kawai, S.i. Towata, T. Matsunaga, T. Shinozawa, M. Kimbara, Journal of Alloys and Compounds, 419 (2006) 256-261.

[25] L. Schlapbach, Hydrogen in Intermetallic Compounds I, (1988).

[26] Y. Fukai, The metal-hydrogen system: basic bulk properties, Springer Science & Business Media, 2006.

[27] Y. Fukai, K. Tanaka, U. Uchida, Hydrogen and Metal, (in Japanese), 1998.

[28] L. Schlapbach, A. Züttel, Nature, 414 (2001) 353.

2 Purpose

As mentioned in the introduction, the development of renewable energy storage technology is important. Among them, we focus on the energy storage technology using nickel-metal hydride (Ni-MH) battery and hydrogen as a stationary energy storage technology for leveling renewable energy. Although Ni-MH battery are required to increase capacity while conserving high efficiency, there is a limit in improvement by the performance of materials. In the case of hydrogen, high efficiency utilization method is required while achieving high capacity. However, its energy efficiency is still lower than that of the secondary battery. Thus, it is necessary to develop the energy storage technology which is high efficiency like Ni-MH battery and has high capacity like hydrogen.

In this research, we study new high capacity and high efficiency energy storage technology combining the technology of Ni-MH battery and hydrogen. We also conduct experiment and discussion to establish its principle. Therefore, "Hybrid Nickel-Metal Hydride/Hydrogen (Ni-MH/H_2) Battery" was proposed as a new concept. This battery is a combination of AB_5-type metal hydride (MH) with high dissociation pressure and a high-pressure hydrogen gas (H_2), as a negative electrode active material. Moreover, this battery is also expected to have higher capacity and higher efficiency than each technique.

Conventionally, AB_5-type MH/hydrogen storage alloys (M) have been studied and developed for utilization as electrode active materials of Ni-MH battery or hydrogen storage materials. Platinum (Pt) has been also generally studied and developed as hydrogen dissociation catalyst of nickel-hydrogen (Ni-H_2) battery or fuel cell on the electrochemical reaction systems. However, in the hybrid negative electrode, the MH play

both above roles. Since the MH electrode is partially soaked into the aqueous electrolyte solution under high-pressure H_2 atmosphere, it is expected that an electrochemical reaction occurs at the solid-liquid interface, and H_2 is absorbed/desorbed at the solid-gas phase interface. The one of important research points is whether MH can be operated at the above interfaces. On the other hand, there is possibility that alloy acts as catalyst for H_2 dissociation like fuel cells. Therefore, whether hydrogen is pass through in the alloy during the charge/discharge processes is another interesting issue in this research.

3 Experimental method

3-1 Sample preparation

Materials

All nominal specification of hydrogen storage alloys is shown in Table 3-1-1 and Table 3-1-2. These alloy were purchased from Japan Metals & Chemicals Co., Ltd.. The samples denoted as "$MmNi_{4.12}Co_{0.79}$" and "$MmNi_{4.19}Co_{0.61}Mn_{0.23}Al_{0.06}$" were used for experiments as the alloys with high hydrogen dissociation pressure.

The mischmetal (Mm) consists of 23.98-25.67 wt.% lanthanum (La), 53.75-53.26 wt.% cerium (Ce), 5.77-5.10 wt.% praseodymium (Pr), and 16.50-15.97 wt.% neodymium (Nd). Atomic ratios of Mm are $La_{0.24}Ce_{0.54}Pr_{0.06}Nd_{0.16}$ and $La_{0.26}Ce_{0.53}Pr_{0.05}Nd_{0.16}$ used for $MmNi_{4.12}Co_{0.79}$ and $MmNi_{4.16}Co_{0.6}Mn_{0.23}Al_{0.05}$, respectively.

These samples were stored and handled in a glove box (MP-P60W, Miwa Manufacturing Co., Ltd.) filled with a purified argon gas (Ar, >99.9999%, Taiyo Nippon Sanso Co.) to prevent as oxidation by air and water.

Table 3-1-1 The weigh and atomic ratio of hydrogen storage alloys.

Lot No.	Weight ratio (wt.%)								Atomic ratio
	La	Ce	Pr	Nd	Ni	Co	Mn	Al	
TL-1064	7.86	17.62	1.89	5.41	56.41	10.81	-	-	$La_{0.24}Ce_{0.54}Pr_{0.06}Nd_{0.16}Ni_{4.12}Co_{0.79}$
SL-3494	8.26	17.14	1.64	5.14	56.33	8.25	2.90	0.34	$La_{0.26}Ce_{0.53}Pr_{0.05}Nd_{0.16}Ni_{4.16}Co_{0.6}Mn_{0.23}Al_{0.05}$

Table 3-1-2 The sample name and hydrogen dissociation pressure of hydrogen storage alloys.

Lot No.	Sample name	Dissociation Pressure (MPa)
TL-1064	$MmNi_{4.12}Co_{0.79}$	2.1
SL-3494	$MmNi_{4.16}Co_{0.6}Mn_{0.23}Al_{0.05}$	0.44

Electrodes

The negative electrode active materials used in this study are hydrogen storage alloys with high hydrogen dissociation pressure such as $MmNi_{4.12}Co_{0.79}$ and $MmNi_{4.16}Co_{0.6}Mn_{0.23}Al_{0.05}$. The alloys were crushed to obtain powder with below 50 μm of particle size (median diameter: 30μm). The $MmNi_{4.12}Co_{0.79}$ alloy was mixed with acrylic resin and carboxymethyl cellulose (CMC) water solution until it was a paste. The paste was coated and dried on a punched Ni current collector. The negative electrode has 3.75wt.% acrylic resin and 1.25wt.% CMC per alloy. The coating amount is 40 mg/cm^2, and circular negative electrode with the diameter of 10 mm was stamped out (estimated capacity: 12.5 mAh) as shown Fig. 3-1-1. The paste including $MmNi_{4.16}Co_{0.6}Mn_{0.23}Al_{0.05}$ was coated on the Ni current corrector using the same method of $MmNi_{4.12}Co_{0.79}$. We also used the negative electrode and the positive electrode including β-$Ni(OH)_2$, with the dimeter of 10 mm obtained by disassembling commercial battery (NP2, Primearth EV Energy Co., Ltd.) as also shown Fig. 3-1-1.

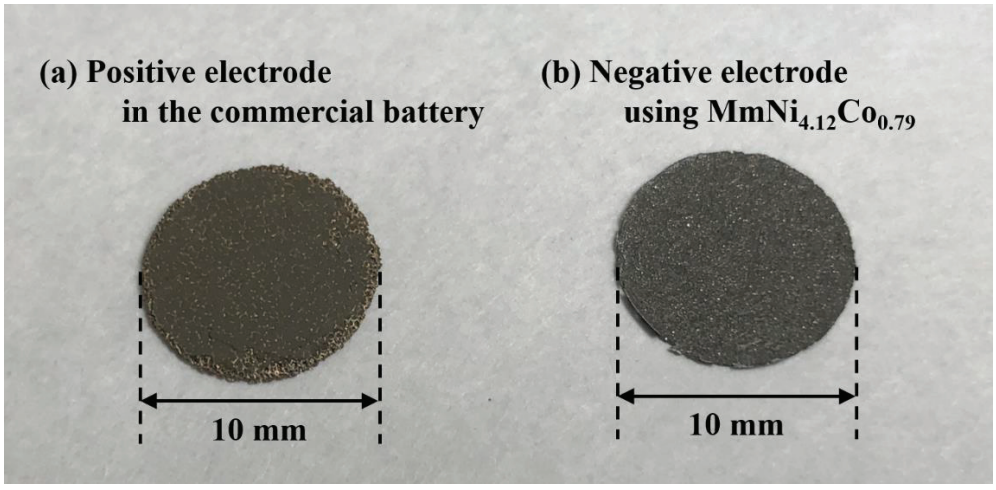

Fig. 3-1-1 Pictures of (a) positive electrode in the commercial battery and (b) negative electrode using $MmNi_{4.12}Co_{0.79}$.

3-2 Pressure-Composition-Temperature measurements

Principle

Pressure-Composition-Temperature (PCT) measurement is a typical technique to evaluate hydrogen absorb/desorb amount and reaction pressure under equilibrium states. There are gravimetric and volumetric methods for PCT measurements. In this study, the volumetric method is used. Fig.3-2-1 shows a schematic diagram of the PCT apparatus. The accurate volume of the parts in this system is measured in advance. The reactor and reservoir are separated by the valve 3, and an inside of the reservoir side is adjusted to a predetermined hydrogen gas pressure. Thereafter, the internal pressure variation is recorded when the valve 3 is opened to connect the reactor and the reservoir. The hydrogen absorb/desorb amount is continuously estimated by these pressure variations.

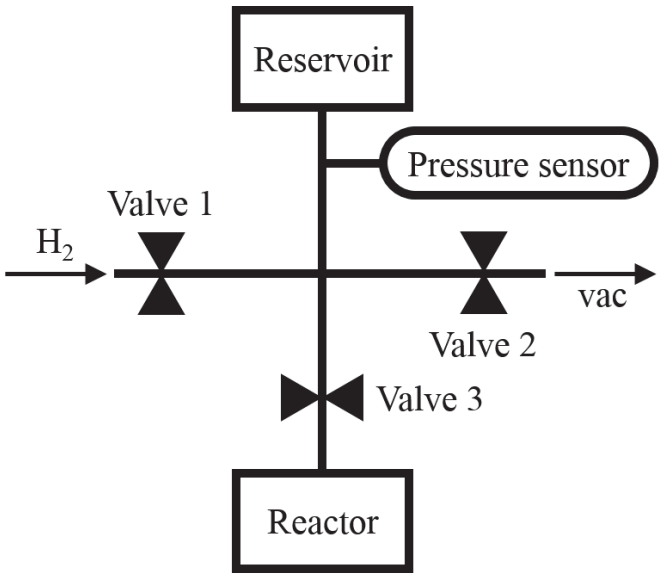

Fig. 3-2-1 Schematic diagram of the PCT apparatus

Procedure

Pressure-composition-isotherms (PCI) experiments were performed for $MmNi_{4.12}Co_{0.79}$, $MmNi_{4.16}Co_{0.6}Mn_{0.23}Al_{0.05}$, and the hydrogen storage alloy used in the commercial Ni-MH battery (NP2, Primearth EV Energy Co., Ltd.). The Sievert's type apparatus manufactured by Suzuki Shokan Co., Ltd. was used for these measurements.

The equilibrium pressure was obtained under variation of each hydrogen pressure of 0.001-5.0 MPa at isothermal condition. The waiting time for stabilization of the pressure in the system was 1 h, and the PCT curves were measured at between 273 K and 373 K. A heater, cooler, and heat insulation vessel containing ice water were used for temperature adjustment. All of PCI were calibrated using blank measurement results.

3-3 High-pressure electrochemical cell

The schematic image of high-pressure electrochemical cell (HP-cell) is shown in Fig. 3-3-1. The cell was specially designed and assembled to investigate the charge-discharge properties under high-pressure hydrogen (H_2, 99.99999%, Taiyo Nippon Sanso Co.) and argon (Ar, 99.99999%, Taiyo Nippon Sanso Co.) atmospheres. The height of the cell is 29.0 cm, the width is 30.5 cm, and the inner volume of the cell is 23.8 cm^3. The pressures were measured by a pressure sensor (520.9K0503L401W, Huba Control), and monitored by digital indicator (KSM801, Krone Co.). The cell capacities of this cell determined by the amount of ß-$Ni(OH)_2$ in the positive electrodes are about 20 mAh. Potassium hydroxide KOH aqueous solution of 30 wt.% (6 $molL^{-1}$) was used with polyolefin separator (thickness: 0.15 mm, Japan Vilene Co., Ltd.). The punched positive electrode with diameter of 10 mm was completely soaked in the KOH aqueous solution to prevent the self-discharge reaction with hydrogen gas directly [1]. The negative electrode with diameter of 10 mm was partially soaked in the KOH aqueous solution so that the surface of the alloy contact with H_2 gas in the same way of the negative electrode of "Nickel-Hydrogen (Ni-H_2) battery" [2] using Pt-based catalyst.

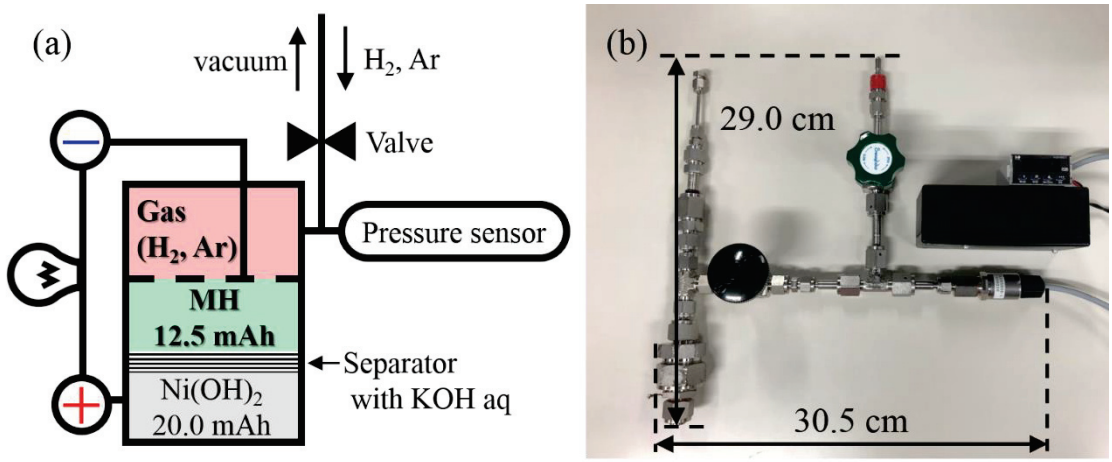

Fig. 3-3-1. (a) Schematic diagram and (b) picture of specially designed high-pressure electrochemical cell (HP-cell).

3-4 Electrochemical measurements

Principle

The charge-discharge measurements are carried out to investigate electrochemical properties of the electrode materials or the battery. For the charge-discharge measurements, there are two types of methods which are the “Constant-Current (CC)” and “Constant-Voltage (CV)” processes. In this study, the electrochemical properties are evaluated by CC charge/discharge technique which is also called the “Chronopotentiometry”. The accurately controlled constant current is applied between the working electrode and the counter electrode, and it provides potential change as a function of time. The capacity (Q) of electrochemical active materials in the electrode are obtained by this measurement as a following equation,

$$\mathrm{Q} = i \times t \tag{3-1}$$

where i is current value, and t is duration time.

Thus, the voltage-time curve is obtained as the “charge-discharge curve”. The vertical axis of this curve is expressed as voltage (V), and its horizonal axis is expressed as specific capacity (mAh/g) or capacity (mAh), which converted from the time according to the above equation. In this equation, the i is the current density per weight or area (mA/g or mA/cm^2) or the current value (mA), and the t is generally hour (h). Additionally, the current value i is often expressed as the capacity rate (C) such as “1 C” or “0.1 C” in the battery field. The “1 C” indicates a current value which is defined as required current to fully charge or discharge the battery in 1 hour. If the current value is "0.1 C", the battery is fully charged or discharged in 10 h.

This curve contains a plateaus feature corresponding to the redox potentials of electrochemical active materials, and it is also possible to estimate the electrochemical reaction potential from the voltage value in the plateau region of the curve.

The chronopotentiometry is performed by using a galvanostat apparatus, which is mainly composed of current supply part and potential recording part. The power supply

part maintains a constant current which is independent of a state of electrochemical active materials in the experimental cell. The potential changes between a working electrode and a counter electrode is observed by the potential recording part.

Procedure

The electrochemical properties of the HP-cell were measured by using charge-discharge test apparatus (HJ1001 SD-8, Hokuto Denko Co.) in the voltage between 1.0 and 1.8 V with current density of 2.54 mA/cm^2 (0.1 C) at 293 K and 253 K by the mixture of sodium chloride (NaCl) and ice. Before the electrochemical measurements, positive and negative electrodes were activated by a charging and discharging under 3.0 MPa H_2 atmosphere. p

3-5 Powder X-ray diffraction

Principle [3]

The X-ray diffraction (XRD) measurement is a technique widely utilized to analyze structural properties, of the sample, such as crystal structure, lattice constant, and atomic position. In this study, the powder XRD is used for phase identification or structure comparison of hydrogen storage alloys and electrodes.

The X-rays used for XRD measurements has a specific wavelength, and this is called “characteristic X-ray”. The electron energy in the atom is quantized and generally classified as the energy level of K, L, M shells in Fig. 3-5-1. The X-ray is generated by irradiating the metal target materials with thermoelectron which is electrically accelerated at high voltage. Then, an electron in the internal energy level are ejected, and an electron in the outer shell fall into a vacant position of the internal shell, with emitting the X-ray to make a stable ground state.

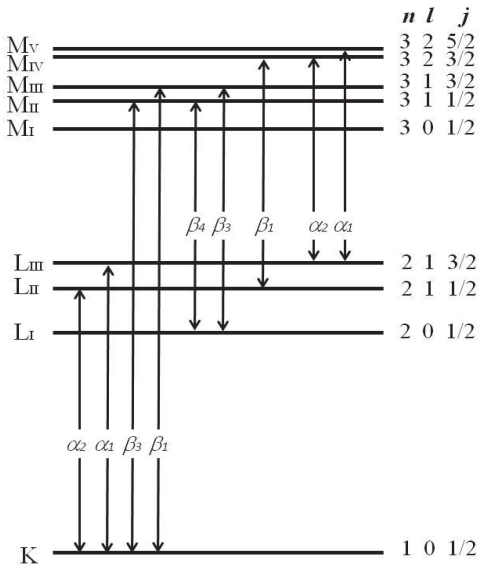

Fig. 3-5-1 Relationship diagram between energy levels of electron shells and characteristic X-rays

This X-ray has a specific wavelength corresponding to the energy difference between the internal and outer shells. The characteristic X-ray has difference in wavelength depending on the target material and the energy level difference. Thus, it is required to select suitable target material and wavelength by considering the composition of samples. Typically, characteristic X-rays of Kα emitted from chromium (Cr), iron (Fe), cobalt (Co), cupper (Cu), and molybdenum (Mo) are utilized for X-ray measurements.

When monochromatic X-ray with a specific wavelength λ such as characteristic X-ray are irradiated at a certain angle θ to the lattice plane, they are diffracted by the electrons of each atom as shown in Fig. 3-5-2. Here, the two lattice planes P1 and P2 with a distance d_{hkl} are assumed in Fig. 3-5-2, in which hkl are miller indexes [4]. The diffracted X-rays are coherent with each other to constructive interference, when the optical path difference is integral multiple "n". This diffraction condition is expressed by the following equation and is well known as the Bragg's law.

$$n\lambda = 2d_{hkl} \sin\theta \tag{3-2}$$

XRD patterns can be obtained by scanning the intensity of the diffracted X-ray with the angle 2θ between the irradiated X-ray and the diffracted X-ray. It is also possible to discuss phase identification and structural change, based on the peak information such as position and intensity ratio, in the XRD pattern.

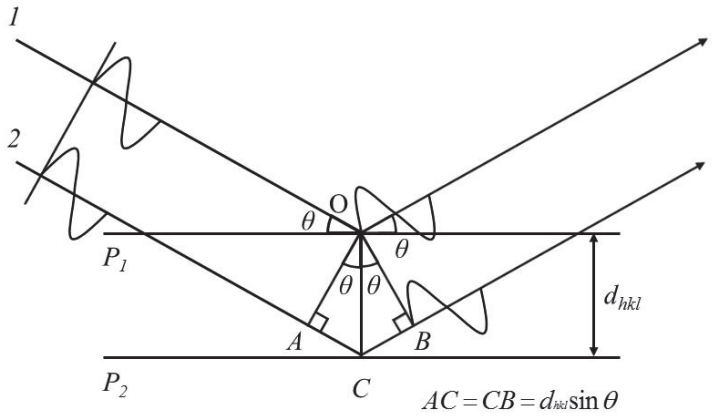

Fig. 3-5-2 Schematic diagrams of scattered wave from lattice plane

Procedure

Powder X-ray diffraction (XRD) measurements were carried out to characterize the structure of hydrogen storage alloys and electrode active materials after charge/discharge. These XRD patterns were measured by RINT-2500V (Rigaku Co.) in which the X-ray source is Cu-Kα (λ=1.54 Å) with 40 kV / 200 mA of output power. These samples were placed on the glass plates and adhered by grease (Apiezon® Grease, M&I Material Ltd.). Additionally, these sample were covered by polyimide sheets (Kapton®, Du Pont-Toray Co., Ltd.) to prevent the exposure to air. All the processes of sample preparation were performed in the glove box. The obtained XRD patterns were analyzed by a software PDXL (Rigaku Co.) with powder diffraction files (PDF) by Joint Committee for Powder Diffraction Standards (JCPDS) as the database.

3-6 Gas chromatography

Principle

The gas chromatography (GC) is an analytical technique which can identify a gaseous species and clarify a molar ratio of mixed gaseous samples.

Generally, an inert gas such as helium (He), nitrogen (N_2), and argon (Ar) is utilized as a carrier gas and the gaseous sample is carried into column packed with a gas adsorbent. The carried sample is separated as each gaseous species by the difference such as weight and adsorption properties according to the principle of a chromatograph, and then they are introduced into the detector part. In this study, Thermal conductivity detector (TCD) is utilized for the detection of gaseous species. This detector electrically counts the amount of each gaseous species according to differences in thermal conductivity between the carrier gas and the gaseous species. Since the sensitivity of TCD depends on the difference in thermal conductivity, it is necessary to select an appropriate carrier gas according to the gaseous sample. The thermal conductivities of typical gaseous species are shown in Table 3-6-1.

Table 3-6-1 Thermal conductivity of each gaseous species

Gaseous species	Thermal conductivity at 273 K (mW/m·K)
Helium (He)	141.5
Hydrogen (H_2)	168.4
Methane (CH_4)	30.1
Ammonia (NH_3)	2.2
Nitrogen (N_2)	24.2
Oxygen (O_2)	24.3
Argon (Ar)	1.5
Carbon dioxide (CO_2)	16.6

The plot of signal strength and time obtained by the GC measurement is called "gas chromatogram". From the obtained gas chromatogram, identification of gaseous species can be achieved by comparing the references, and the molar ratio of the gas species contained in the sample can be estimated by analyzing peak area using calibration date of the standard sample.

Procedure

The released gas from electrodes during charging at 0.10 MPa Ar atmosphere, was analyzed by gas chromatography system (GC-14B, Shimadzu Co., Ltd.). High purity H_2 (99.99999%, Taiyo Nippon Sanso Co.) and O_2 (99.999%, Taiyo Nippon Sanso Co.) were also measured by GC as standard samples. Ar was used as carrier gas at the pressure of 120 kPa. The packing absorbent in the column was Shicarbon ST, and the column was heated at 373 K during the measurements. Other parts such as injection and TCD detector were heated at 393 K.

Reference

[1] Z. Mao, A. Visintin, S. Srinivasan, A.J. Appleby, H.S. Lim, Journal of Applied Electrochemistry, 22 (1992) 409-414.

[2] L.H. Thaller, A.H. Zimmerman, in, 2003.

[3] Y. Waseda, E. Matsubara, UHIDA ROKAKUHO PUBLISHING CO., LTD., (1998).

[4] K. Asakura, Powder X-ray analysis no zissai, Asakura Publishing Co, Ltd., 2002.

4. Result & Discussion

4-1 Concept of "Nickel-Metal Hydride/Hydrogen Battery"

Conceptive picture of the "Hybrid Nickel-Metal Hydride/Hydrogen (Ni-MH/H_2) Battery" is shown in Fig. 2. This battery consists of positive electrode using $Ni(OH)_2$ as an active material and hybrid negative electrode, which is composed of hydrogen storage alloy with high hydrogen dissociation pressure (M) and high-pressure hydrogen gas (H_2) as active materials. The dissociation pressure of the M at plateau region is above 0.1 MPa and the gravimetric hydrogen density is 1.4-1.5 wt.% [1]. These M has a higher gravimetric hydrogen density than the hydrogen storage alloy with low dissociation pressure less than 0.1 MPa, used for commercial batteries (~ 1.1 wt.%). However, these metal hydride states (MH) are unstable under atmospheric pressure, due to their high dissociation pressure. Thus, these MH had not been studied as active materials for commercial Ni-MH battery application. In this concept, these MHs are stabilized by using high-pressure H_2 atmosphere. Additionally, by contributing H_2 as in the atmosphere as a negative electrode material, it is expected to realize a high capacity negative electrode combined with these MH.

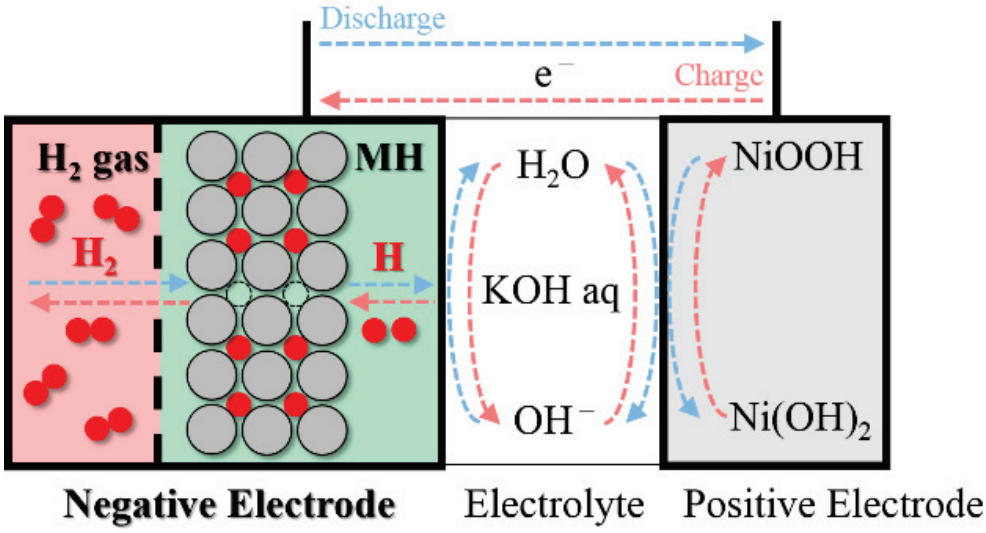

Fig. 4-1-1 Conceptive picture of "Hybrid Nickel-Metal Hydride/Hydrogen (Ni-MH/H_2) battery".

Although the positive electrode reaction is identical with the commercial Ni-MH battery as follows,

$$Ni(OH)_2 \rightleftarrows NiOOH + H_2O + e^-, \quad (4\text{-}1)$$

the reaction of negative electrode is divided into two reactions. One reaction represents hydrogen insertion and deinsertion in the alloy,

$$M + H_2O + e^- \rightleftarrows MH + OH^-. \quad (4\text{-}2)$$

The other reaction represents H_2 is desorbed and absorbed with the charging and discharging due to the above reaction in the vessel, respectively,

$$M + \frac{1}{2}H_2 \rightleftarrows MH. \quad (4\text{-}3)$$

Hydrogen corresponding to the capacity of M is electrochemically inserted at the charge process, and M is changed to MH. Subsequently, the excess hydrogen which compared with the capacity of M is released as a gas. On the other hand, at the discharge process, hydrogen is electrochemically released from the MH and M is formed. Simultaneously, M absorbs gaseous H_2 in the atmosphere and is formed to MH. Thus, in this concept, it is key issues whether gaseous hydrogen will reversibly be formed/consumed on the charge/discharge reaction through inside of the alloy.

The AB_5-type alloy with high dissociation pressure leads large volumetric capacity of 3200-3400 $mAhcm^{-3}$ assuming that the density is 8.6 gcm^{-3} [1], while the calculated gravimetric capacity is 370-400 mAh/g according to a general method in the reference [2]. However, high-pressure H_2 has large gravimetric capacity of 26,600 mAh/g, while the volumetric capacities at 293 K are 629 $mAhcm^{-3}$ (0.0237 gcm^{-3}), 475 $mAhcm^{-3}$ (0.0179 gcm^{-3}), and 207 $mAhcm^{-3}$ (0.00780 gcm^{-3}) under 35 MPa, 25 MPa, and 10 MPa, respectively [3]. Thus, for this hybrid battery, the gravimetric energy densities of Ni-MH can be controlled and improved by changing the molar ratio of the alloy and compressed hydrogen gas under various pressure.

We have calculated theoretical capacities of the hybrid Ni-MH/H_2 battery combining the AB_5-type alloy with high dissociation pressure and high-pressure H_2 under several pressures, 35 MPa, 20 MPa, and 10 MPa. It is assumed that the container of the negative electrode which is composed a AB_5-type alloy with high dissociation pressure including high-pressure H_2 is 10 L, and the density of this alloy is 8.6 gcm^{-3}. Assuming

that filling ratio of the alloy powder is 50%, the volumetric packing ratio of the alloy to hydrogen is adjusted in the range of 0 to 50% (weight of the alloy: 0 to 43 kg), in the container. Additionally, we have also calculated theoretical capacity of the commercial Ni-MH battery, which is composed of a AB_5-type alloy with high dissociation pressure. It is assumed that the density of this alloy is assumed to be 8.0 gcm^{-3}, and filling ratio of the alloy powder is also 50% as described above.

Fig. 4-1-2 shows the gravimetric capacities C_{ng} and volumetric capacities, C_{nv} of the negative electrode in this hybrid battery under 35 MPa of H_2, at 293 K.

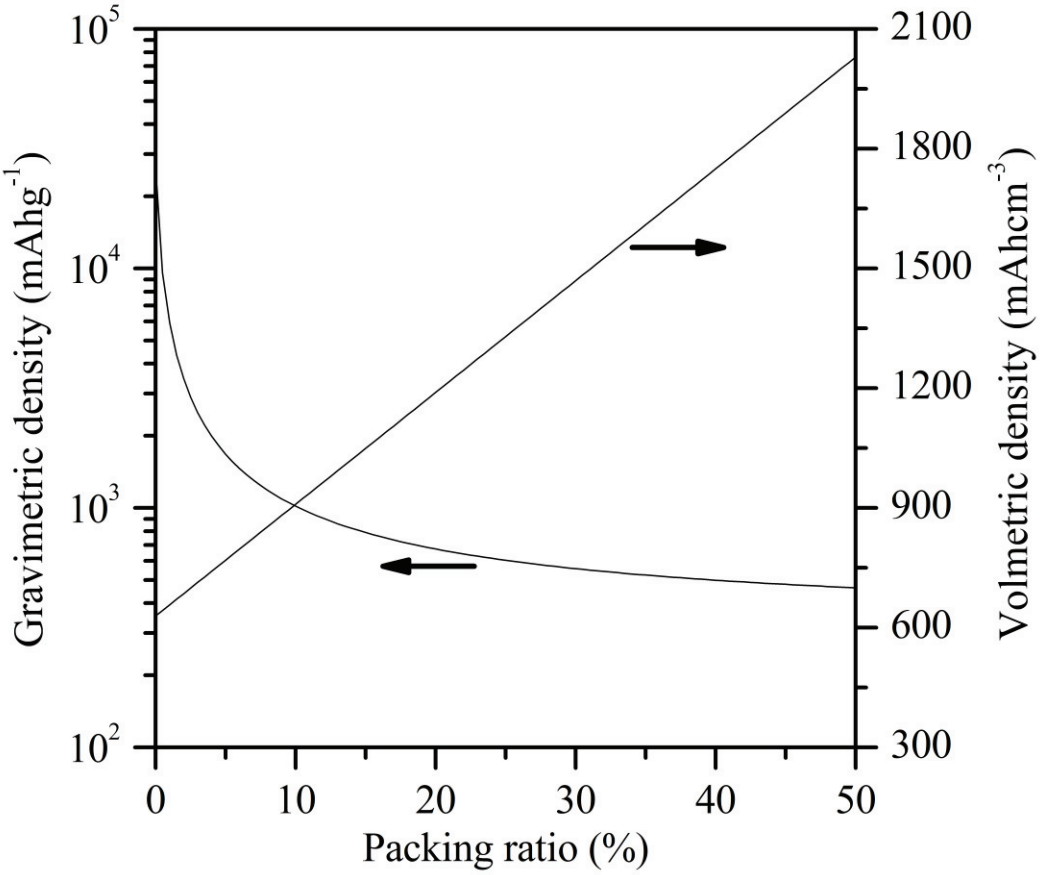

Fig. 4-1-2 The dependences of gravimetric/volumetric densities on packing ratio, under 35 MPa of H_2, at 293 K.

The C_{ng} decreases with the packing ratio and has 471 $mAhg^{-1}$ at 50%. The C_{nv} increase linearly with the packing ratio of the alloy and has 2030 $mAhcm^{-3}$ at 50%. The C_{ng} and C_{nv} of a negative electrode in this hybrid battery under 35 MPa are 801 $mAhg^{-1}$ and 1049 $mAhcm^{-3}$, respectively. Here, the packing ratio of the AB_5-type alloy with high dissociation pressure to high-pressure H_2 is 15%. This C_{ng} is about 2.7 times the C_{ng} of a AB_5-type alloy used as negative electrode material in the commercial batteries (292 $mAhg^{-1}$), while the C_{nv} is similar value to a negative electrode in the commercial batteries using AB_5-type alloy (1170 $mAhcm^{-3}$).

Fig. 4-1-3 shows the gravimetric capacities C_{ng} and volumetric capacities, C_{nv} of the negative electrode in this hybrid battery under 20 MPa of H_2, at 293 K.

The C_{ng} decreases with the packing ratio and has 444 $mAhg^{-1}$ at 50%. The C_{nv} increase linearly with the packing ratio of the alloy and has 1910 $mAhcm^{-3}$ at 50%. In which the packing ratio is 22%, the value of C_{nv} is equivalent to that of commercial batteries, and the value of C_{ng} is about 1.9 times that of commercial batteries. The C_{ng} and C_{nv} are 557 mAh/g and 1060 mAh/cm^3, respectively.

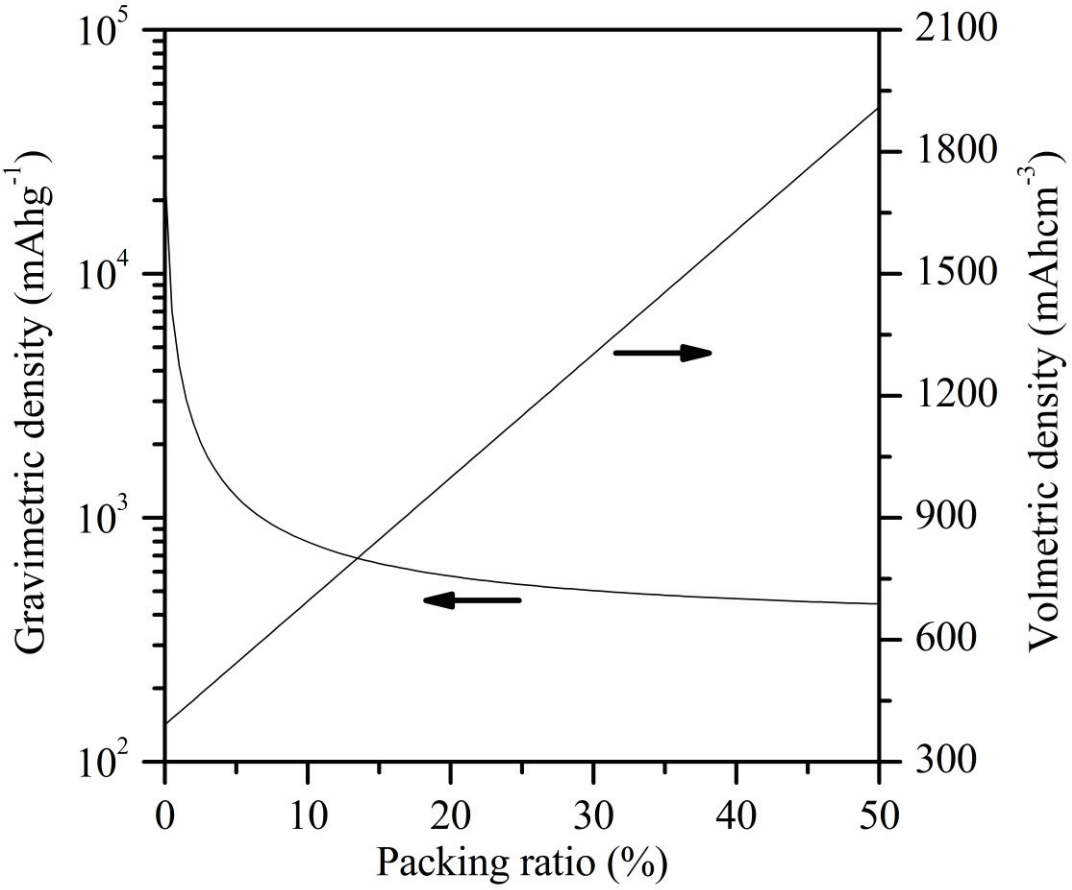

Fig. 4-1-3 The dependences of gravimetric/volumetric densities on packing ratio, under 20 MPa of H_2, at 293 K.

Fig. 4-1-4 shows the gravimetric capacities C_{ng} and volumetric capacities, C_{nv} of the negative electrode in this hybrid battery under 10 MPa of H_2, at 293 K.

The C_{ng} decreases with the packing ratio and has 423 $mAhg^{-1}$ at 50%. The C_{nv} increase linearly with the packing ratio of the alloy and has 1819 $mAhcm^{-3}$ at 50%. In which the packing ratio is 26%, the value of C_{nv} is equivalent to that of commercial batteries, and the value of C_{ng} is about 1.6 times that of commercial batteries. The C_{ng} and C_{nv} are 466 mAh/g and 1045 $mAhcm^{-3}$, respectively.

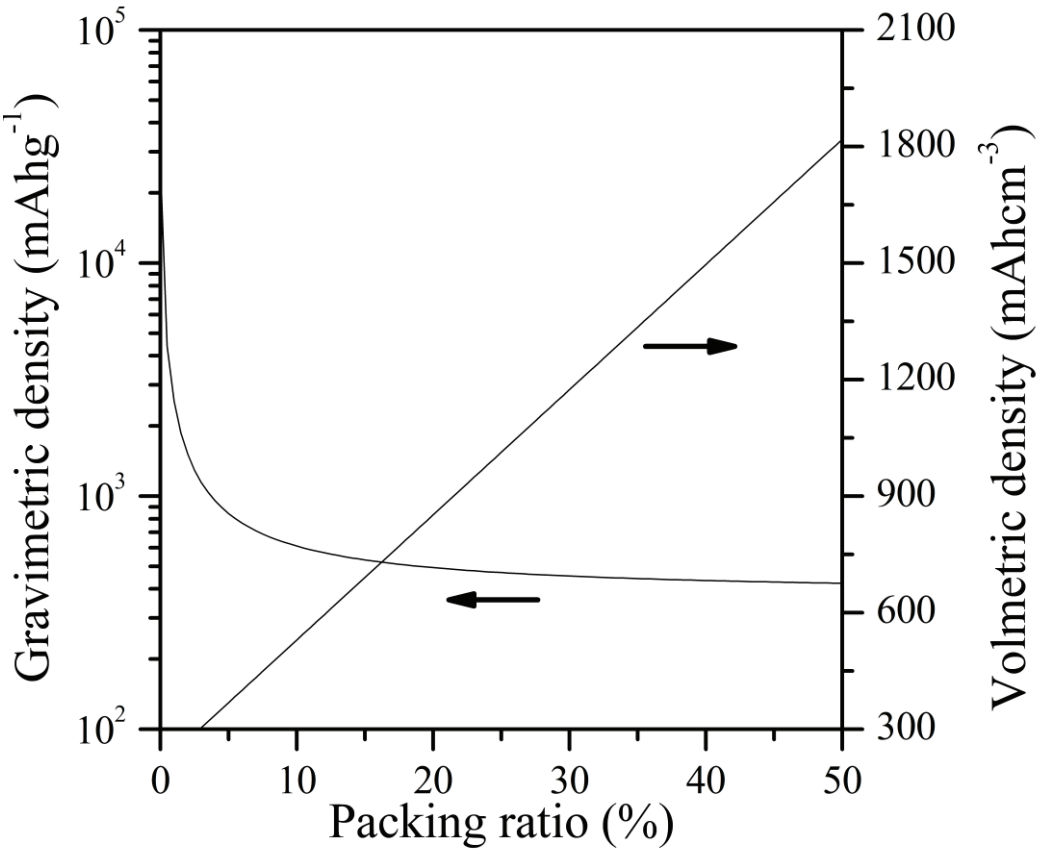

Fig. 4-1-4 The dependences of gravimetric/volumetric densities on packing ratio, under 10 MPa of H_2, at 293 K.

Assuming that the capacity of the negative electrode active materials are equal to positive electrode active materials [4], then, gravimetric and volumetric energy densities E_g (Whkg^{-1}), E_v (WhL^{-1}) of the battery are expressed by the following equation

$$E_g = \frac{1.3C_{ng}}{\frac{92.7C_{ng}}{26800}+1} \tag{4-4}$$

$$E_v = \frac{1.3C_{nv}}{\frac{92.7C_{nv}\ \ 1}{26800\ \ 2.08}+1} \tag{4-5}$$

Here, we used battery voltage of 1.3 V. The C_{ng} and C_{nv} are determined as described above under 35, 20, and 10 MPa of H_2. Molecular weight of $Ni(OH)_2$ is 92.7 and the quantity of electricity per electron is 26800 $mAhmol^{-1}$. The packing density of $Ni(OH)_2$ is 2.08 gcm^{-3}, by assuming that the packing ratio is 50%. We have calculated the E_g and E_v of hybrid Ni-MH/H_2 battery and commercial Ni-MH battery according to equations (4-4), (4-5). Table 4-1-1 shows energy densities of these batteries without binder, electrolyte, current collector, separator and vessel.

Table 4-1-1 Calculated gravimetric/volumetric energy densities (E_g/E_v) of the hybrid Ni-MH/H_2 battery and commercial Ni-MH batteries.

Energy density	Hybrid Ni-MH/H_2 battery			Commercial Ni-MH battery
	35 MPa	20 MPa	10 MPa	
E_g ($Whkg^{-1}$)	275	246	231	190
E_v (WhL^{-1})	497	499	496	519

The gravimetric density increases up to 1.5 times, although the volumetric density has similar value, under 35 MPa of H_2. The required amount of AB_5-type alloys in the hybrid battery decreases down to 32 wt.% compared with the Ni-MH battery. As a result, the amount of rare-earth element can be decreased.

4-2 Characterization of electrode materials

Fig. 4-2-1 shows powder X-ray diffraction (XRD) pattern of a positive electrode in the commercial battery. XRD pattern of this electrode shows peaks at 2θ of 19.03, 33.09, 38.51, 59.07, and 62.67˚. These peaks originate in (001), (100), (101), (110), and (111) planes of ß-Ni(OH)$_2$ having Cd(OH)$_2$ type hexagonal structure (space group: P-3m1) [5]. The interlayer distance of ß-Ni(OH)$_2$ is 4.72 Å which is calculated by 2θ of (001) peak according to the Bragg's law.

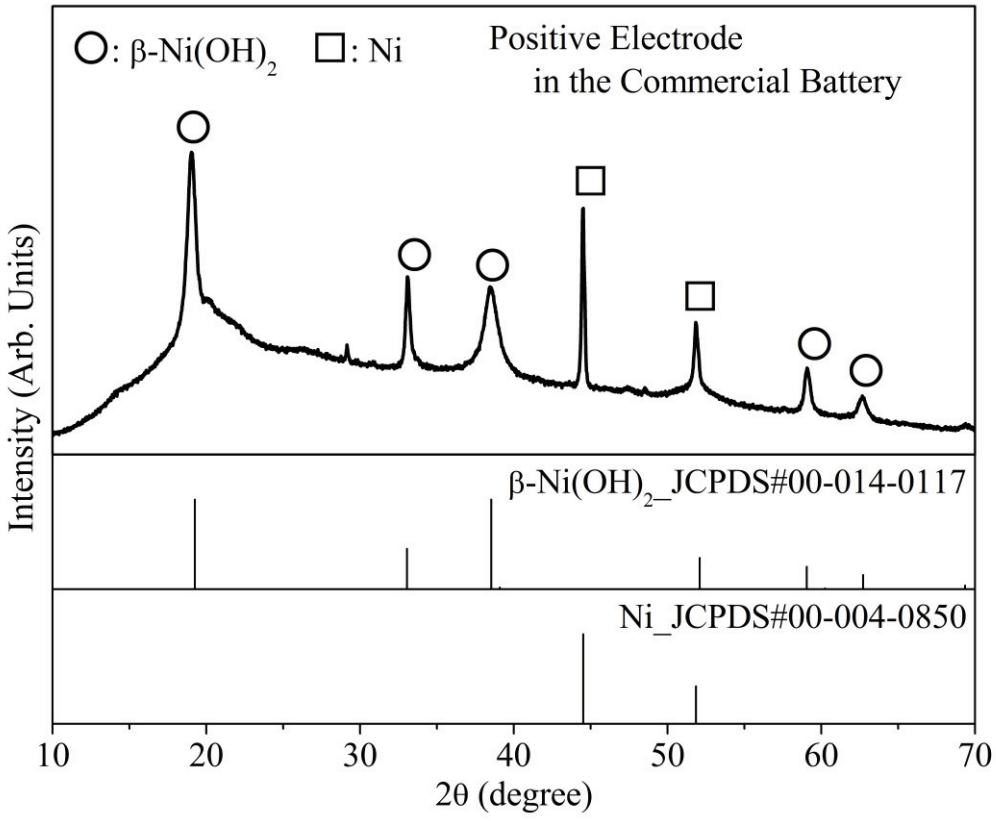

Fig. 4-2-1 XRD pattern of a positive electrodes in the commercial battery with the data of β-Ni(OH)$_2$ (JCPDS file No. 00-014-0117) and Ni (JCPDS file No. 00-004-0850).

Fig. 4-2-2 shows XRD patterns of $MmNi_{4.12}Co_{0.79}$, $MmNi_{4.16}Co_{0.6}Mn_{0.23}Al_{0.05}$, and a hydrogen storage alloy used to the commercial Ni-MH batteries. The XRD patterns indicates that These alloys has hexagonal $CaCu_5$ type crystal structure (space group: P6/mmm) [6] [7], which is similar to AB_5-type alloys such as $LaNi_5$ (JCPDS file No. 00-055-0277).

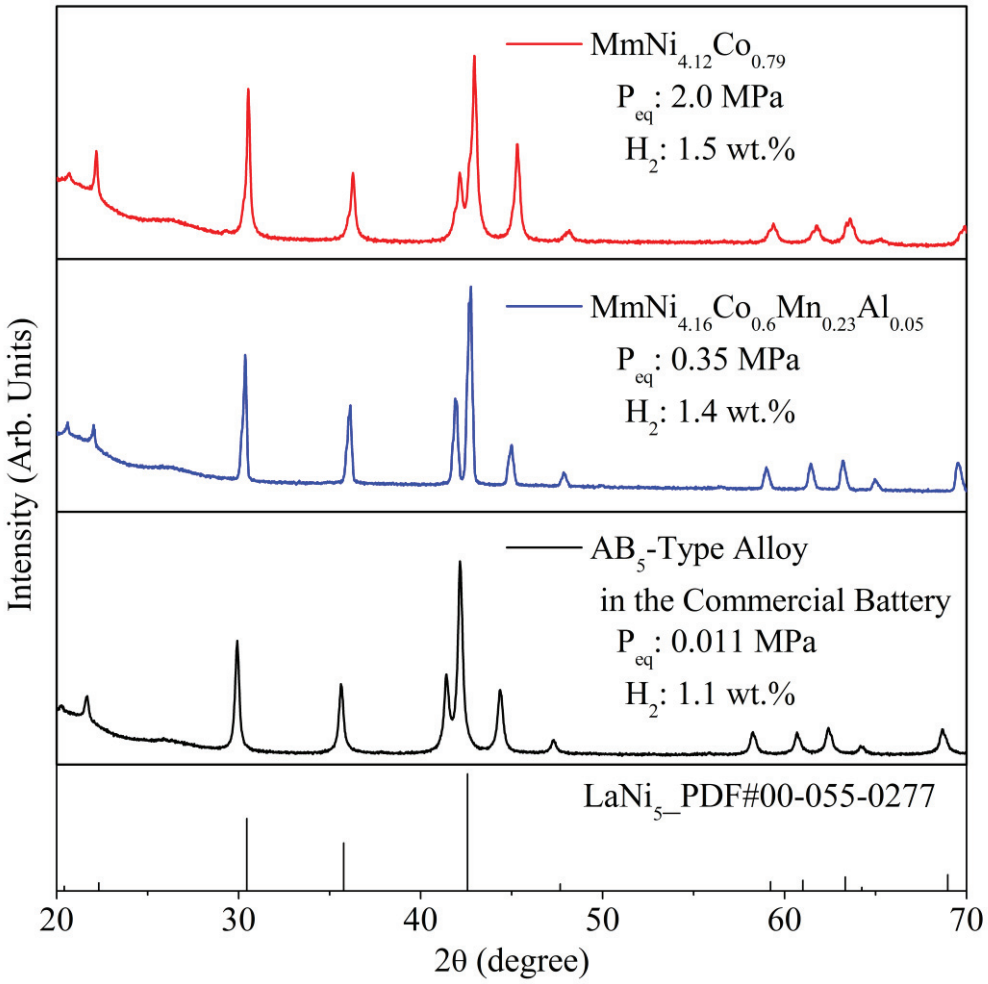

Fig. 4-2-2 XRD patterns of (red) $MmNi_{4.12}Co_{0.79}$, (blue) $MmNi_{4.16}Co_{0.6}Mn_{0.23}Al_{0.05}$, and (black) hydrogen storage alloy in the commercial batteries together with the JCPDS data of $LaNi_5$ (JCPDS file No. 00-055-0277).

The peaks of $MmNi_{4.12}Co_{0.79}$ and $MmNi_{4.16}Co_{0.6}Mn_{0.23}Al_{0.05}$ are shifted to high angle side compared with the peaks of $LaNi_5$. This phenomenon suggests that the lattice constants of these alloys are smaller than the value of $LaNi_5$. On the other hand, the peaks of AB_5-type alloy in the commercial battery are shifted low angle side compared with the peaks of $LaNi_5$. This phenomenon suggests that the lattice constants of these alloys are higher than the value of $LaNi_5$. The lattice constants and cell volumes of these alloys are shown in Table 4-2-1.

Table 4-2-1. The lattice constants (a_0, c_0) and cell volumes of $MmNi_{4.12}Co_{0.79}$, $MmNi_{4.16}Co_{0.6}Mn_{0.23}Al_{0.05}$, AB_5-type alloy in the commercial battery, and $LaNi_5$ (JCPDS file No. 00-055-0277).

Alloy	Lattice constant (Å)		Lattice volume (Å^3)
	a_0	c_0	
$MmNi_{4.12}Co_{0.79}$	4.84	4.06	82.3
$MmNi_{4.16}Co_{0.6}Mn_{0.23}Al_{0.05}$	4.97	3.94	84.2
AB_5-type alloy in the commercial batteries	5.04	3.97	87.2
$LaNi_5$ (JCPDS file No. 00-055-0277)	5.02	3.98	86.7

Fig. 4-2-3 shows pressure composition isotherm (PCI) for hydrogen desorption process of $MmNi_{4.12}Co_{0.79}$ and $MmNi_{4.16}Co_{0.6}Mn_{0.23}Al_{0.05}$ at 293 K. The PCI of AB_5-type alloy used to the commercial Ni-MH batteries is also shown as a reference in Fig. 4-2-2. The plateau dissociation pressures were obtained by an equilibrium pressure at desorbing hydrogen which is 50% of the maximum absorbed hydrogen amount [1]. The dissociation pressure of $MmNi_{4.12}Co_{0.79}$ and $MmNi_{4.16}Co_{0.6}Mn_{0.23}Al_{0.05}$ are 2.0 MPa and 0.35 MPa at

293 K, respectively. These pressures have higher than that of AB_5-type alloys in the commercial batteries (0.012 MPa at 293 K). It has been reported that the dissociation pressure of AB_5-type alloys increases with decreasing of the cell volume [2] [8] [9]. $MmNi_{4.12}Co_{0.79}$, $MmNi_{4.16}Co_{0.6}Mn_{0.23}Al_{0.05}$, and AB_5-type alloy in the commercial batteries also follow the trend as shown in Fig. 4-2-4.

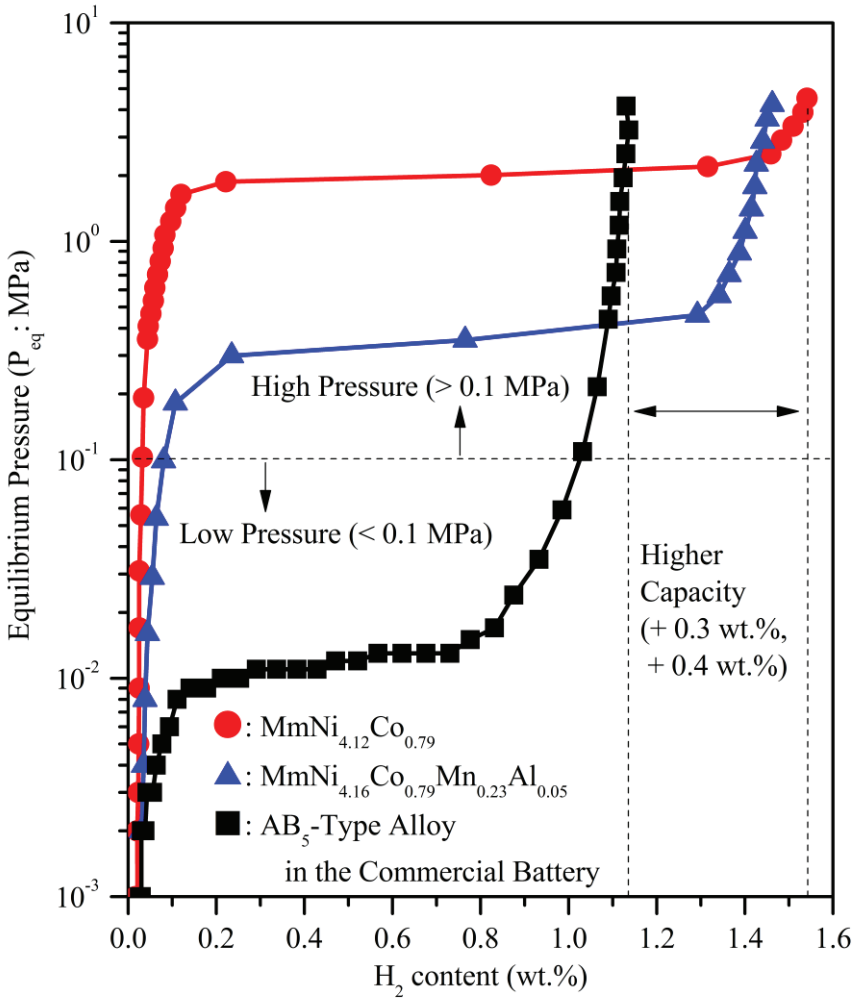

Fig. 4-2-3 Dissociation pressure composition isotherms (PCIs) of (●) $MmNi_{4.12}Co_{0.79}$, (▲)$MmNi_{4.16}Co_{0.6}Mn_{0.23}Al_{0.05}$, and (■) AB_5-type alloy in the commercial batteries at 293 K.

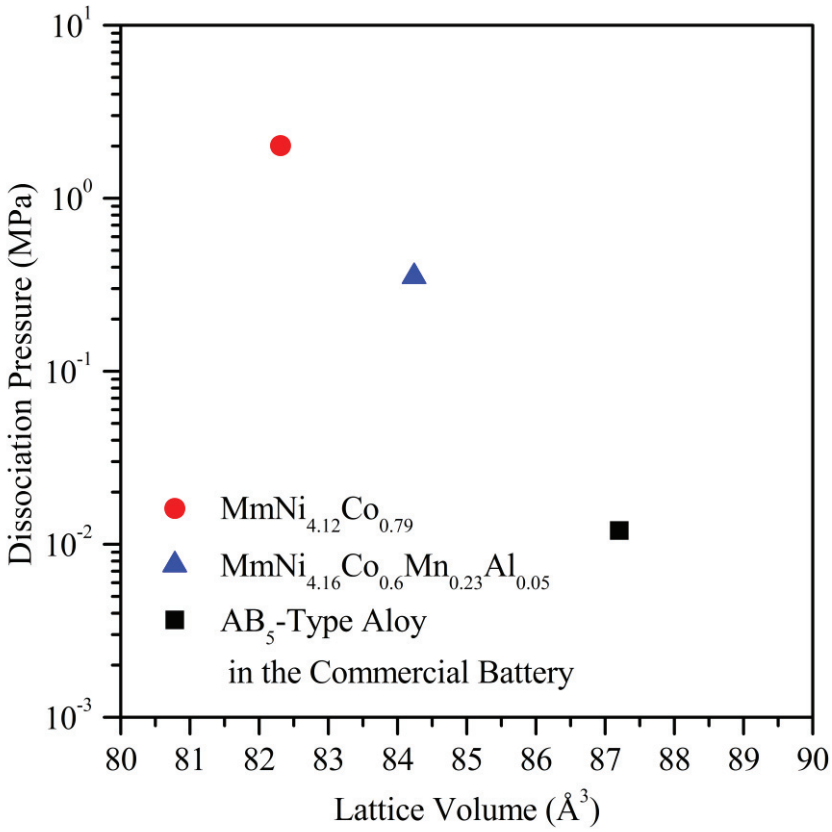

Fig. 4-2-3 The dependence of the dissociation pressure on lattice volume in AB_5-type alloy parameters.

The reversible hydrogen capacity of $MmNi_{4.12}Co_{0.79}$ is 1.5 wt.% between 5 and 10^{-3} MPa of H_2. Theoretically calculated electrochemical capacity was 405 mAh/g. This capacity was higher than a value of the AB_5-type alloy in commercial battery (1.1 wt.%, 294 $mAhg^{-1}$). The reversible hydrogen capacity of $MmNi_{4.16}Co_{0.6}Mn_{0.23}Al_{0.05}$ is 1.4 wt.% between 5 and 10^{-3} MPa of H_2. Theoretically calculated electrochemical capacity was 381 mAh/g. This capacity is also higher than a value of the AB_5-type alloy in commercial battery.

The standard enthalpy change (ΔH) and the standard entropy change (ΔS) of hydrogen desorption reactions were estimated by van't Hoff equation shown in equation (4) [10] [11].

$$\ln \frac{P_{\mathrm{eq}_{\mathrm{H_2}}}}{\mathrm{P}^0} = \frac{\Delta H}{\mathrm{R}T} - \frac{\Delta S}{\mathrm{R}} \tag{4-6}$$

where $P_{\mathrm{eq}_{\mathrm{H_2}}}$ is the dissociation pressure of hydrogen storage alloy (MPa), P^0 is standard pressure (0.101 MPa), R is gas constant (8.314 J $K^{-1}mol^{-1}$), T is temperature (K).

Fig. 4-2-5 shows the dissociation pressure composition temperature (PCT) curves and van't Hoff plot of $MmNi_{4.12}Co_{0.79}$ at 293 K, 283 K, and 273 K. The standard enthalpy change (heat of formation) ΔH and the standard entropy change ΔS of $MmNi_{4.12}Co_{0.79}$ are -25.4 kJmol-H_2^{-1} and -111 JK^{-1}mol-H_2^{-1}, respectively.

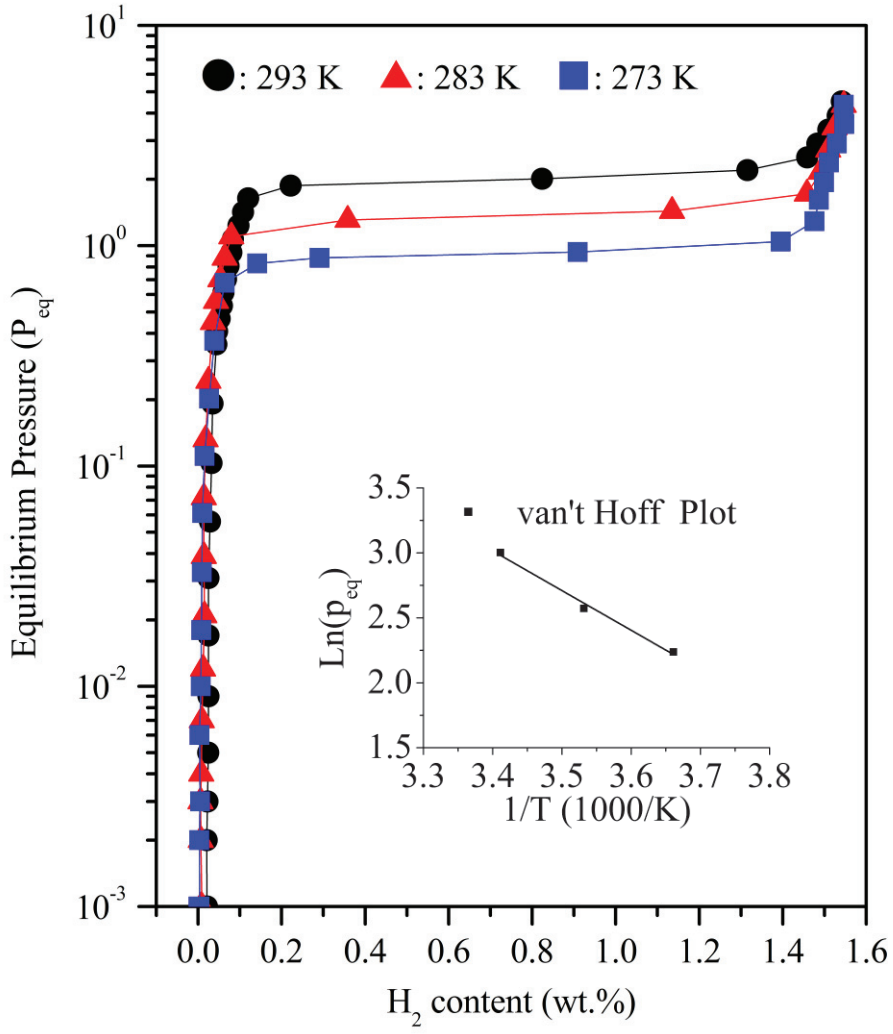

Fig. 4-2-5 Dissociation pressure composition temperature (PCT) curves and van't Hoff plot of $MmNi_{4.12}Co_{0.79}$ at 293 K, 283 K, and 273 K.

Fig. 4-2-6 also shows the PCT curves and van't Hoff plot of $MmNi_{4.16}Co_{0.6}Mn_{0.23}Al_{0.05}$ at 293 K, 303 K, and 313 K. The ΔH and the ΔS of $MmNi_{4.16}Co_{0.6}Mn_{0.23}Al_{0.05}$ were -30.5 kJmol-H_2^{-1} and -115 JK^{-1}mol-H_2^{-1}, respectively.

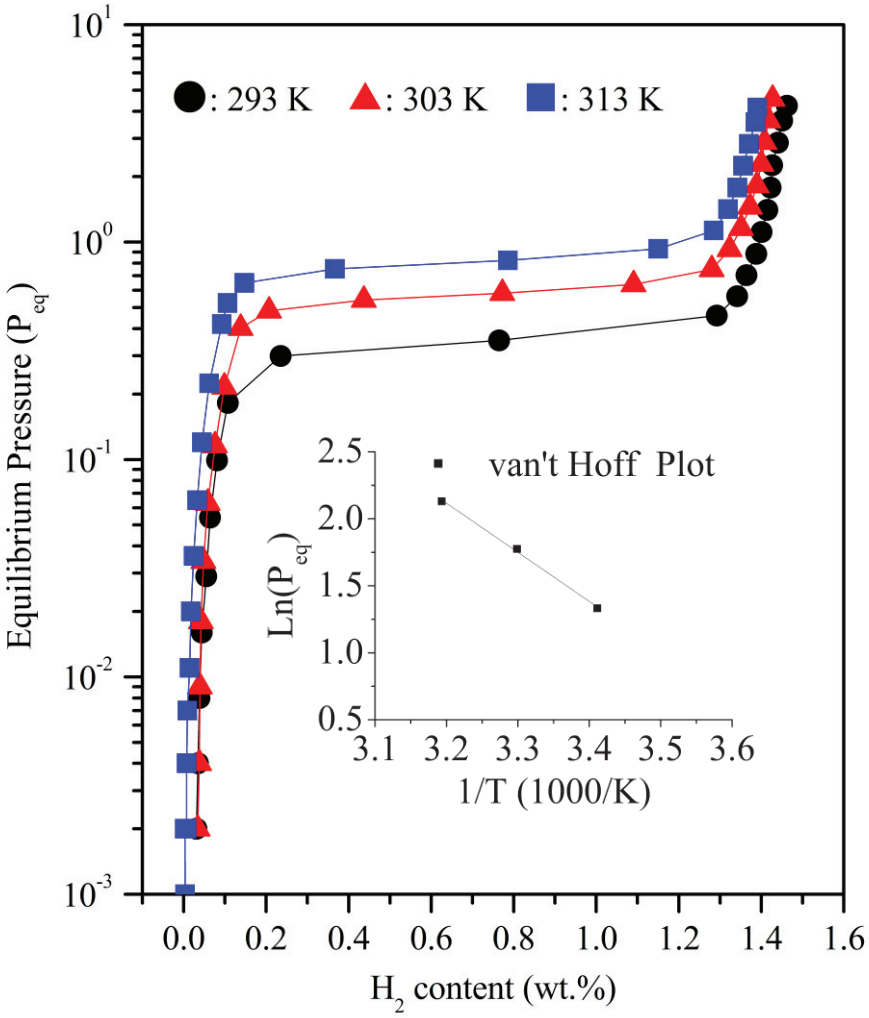

Fig. 4-2-6 Dissociation pressure composition temperature (PCT) curves and van't Hoff plot of $MmNi_{4.16}Co_{0.6}Mn_{0.23}Al_{0.05}$ at 293 K, 303 K, and 313 K.

These absolute ΔH values of $MmNi_{4.12}Co_{0.79}$ and $MmNi_{4.16}Co_{0.6}Mn_{0.23}Al_{0.05}$ are small compared with the AB_5-type alloy used for the commercial Ni-MH batteries, which is calculated by the PCT curves and van't Hoff plots as shown Fig. 4-2-7 (ΔH: -34.8 kJmol-H_2^{-1}). These absolute ΔS values of $MmNi_{4.12}Co_{0.79}$ and $MmNi_{4.16}Co_{0.6}Mn_{0.23}Al_{0.05}$ are high compared with the AB_5-type alloy used for the commercial Ni-MH batteries (ΔS:

-101 J K^{-1}mol-H_2^{-1}). Additionally, All of absolute ΔS values are smaller than entropy of H_2 (131 J K^{-1}mol-H_2^{-1}) [3].

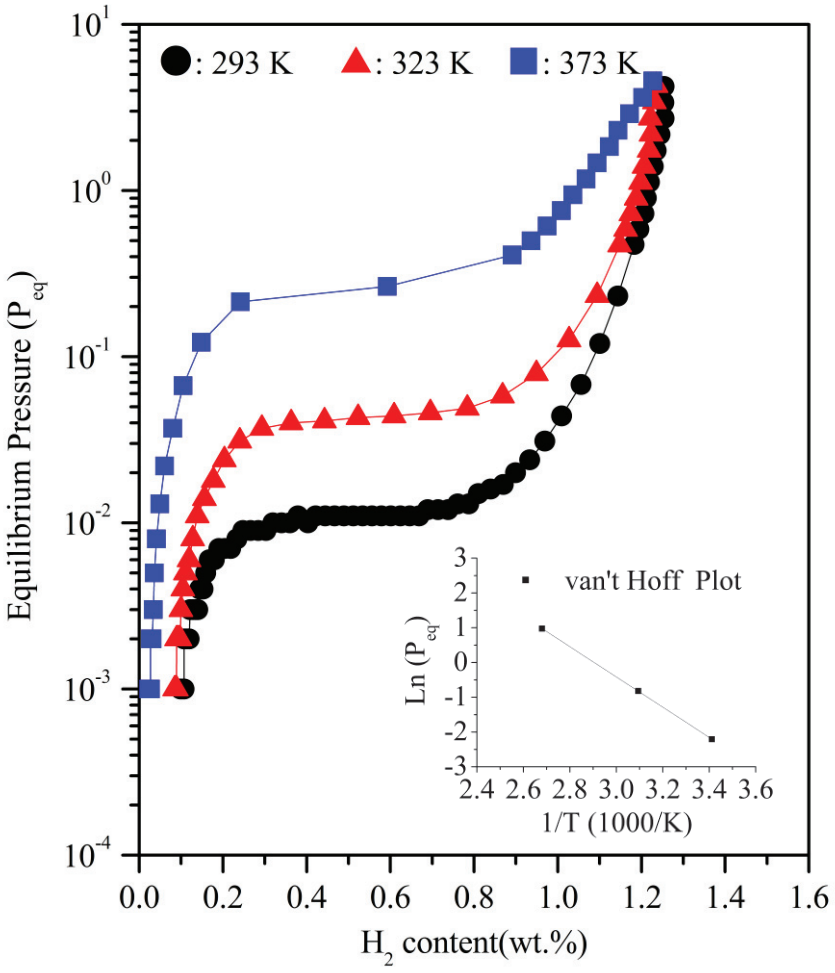

Fig. 4-2-7 Dissociation pressure composition temperature (PCT) curves and van't Hoff plot of AB_5-type alloy in the commercial battery at 293 K, 323 K, and 373 K.

4-3 Charge/Discharge properties of the high-pressure electrochemical cell

Fig. 4-3-1 shows charge/discharge curves of the high-pressure electrochemical cell (HP-cell) which composed of ß-$Ni(OH)_2$ positive electrode and $MmNi_{4.12}Co_{0.79}$ negative electrode under H_2 of 3.0 MPa which is above the dissociation pressure of the alloy. All the charge experiment is carried out up to the capacities of 20 mAh which is determined by theoretical capacity of the ß-$Ni(OH)_2$ electrode in the HP-cell.

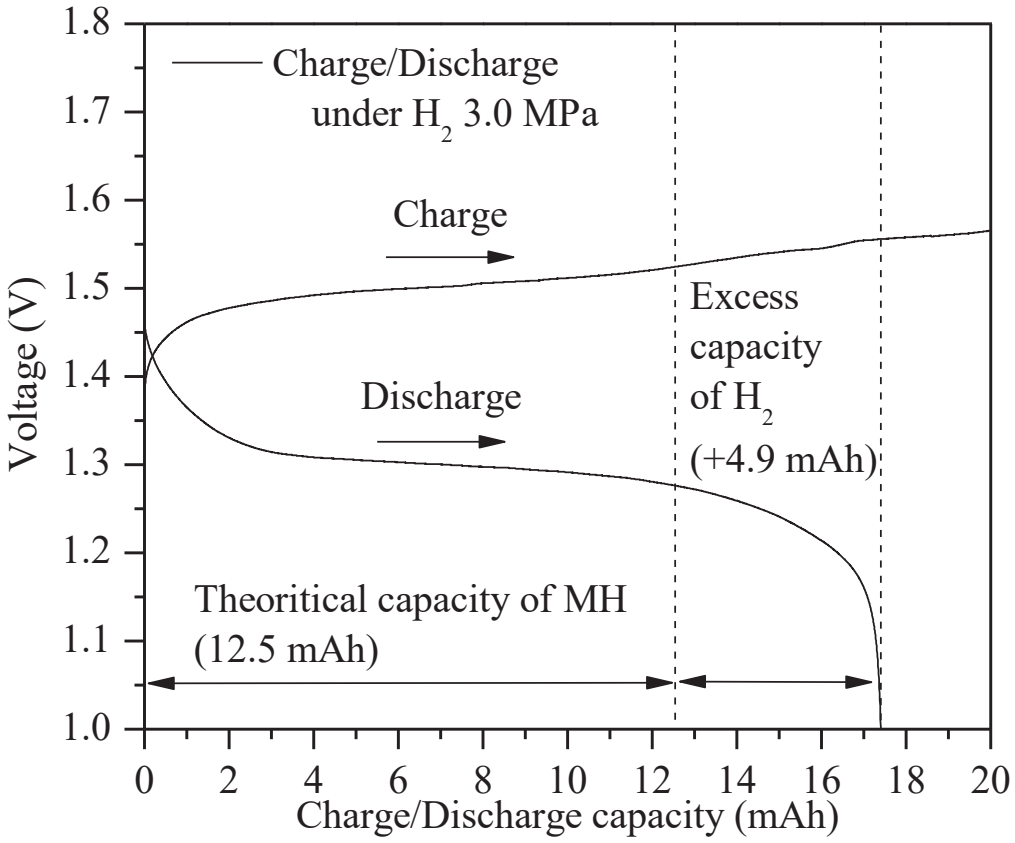

Fig. 4-3-1 Charge and discharge curves of HP-cell using $MmNi_{4.12}Co_{0.79}$ as a negative electrode material with current density of 2.54 $mAcm^{-2}$ (0.1 C) at 293 K, under 3.0 MPa of H_2.

The discharge capacity is 17.4 mAh, which includes an excess discharge capacity of 4.9 mAh, although the theoretical capacity of $MmNi_{4.12}Co_{0.79}$ electrode was

12.5 mAh without gaseous H_2. Namely, it is suggested that the gaseous H_2 can be utilized as the electrode active material in the discharging process.

Fig. 4-3-2 shows charge/discharge curves of HP-cell composed of ß-$Ni(OH)_2$ electrode and $MmNi_{4.12}Co_{0.79}$ electrode under H_2 of 3.0 MPa on different KOH aqueous solution amount.

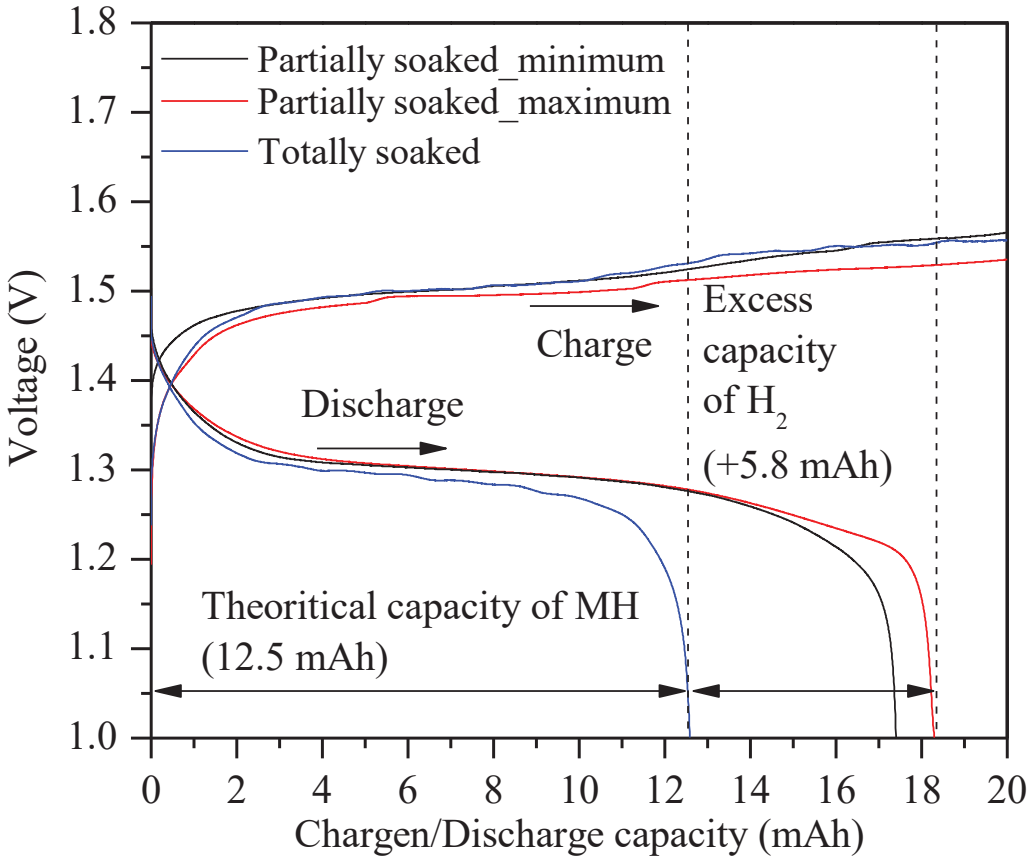

Fig. 4-3-2 Charge/discharge curves of HP-cell using $MmNi_{4.12}Co_{0.79}$ as a negative electrode material with current density of 2.54 $mAcm^{-2}$ (0.1 C) at 293 K, under 3.0 MPa of H_2, on the several KOH aqueous solution amounts.

The discharge capacity is changed from 17.4 to 18.3 mAh as shown in Fig. 4-3-2 on partially soaking (0.1 mL) of the $MmNi_{4.12}Co_{0.79}$ electrode in KOH aqueous solution, at repeated charge /discharge measurements. The capacity was down to 12.5 mAh by totally

soaking the $MmNi_{4.12}Co_{0.79}$ electrode in KOH aqueous solution. This capacity corresponds to the theoretical capacity estimated form the amount of $MmNi_{4.12}Co_{0.79}$, and the excess capacity by gaseous H_2 is not observed. These results indicate that the dried interface for reaction between alloy and gaseous H_2 is necessary to utilize the H_2 gas for the electrochemical reaction.

Fig. 4-3-3 shows charge curves of the high-pressure electrochemical cell (HP-cell) composed of ß-$Ni(OH)_2$ and $MmNi_{4.12}Co_{0.79}$ electrodes under H_2 of 1.0 and 3.0 MPa which is below and above the dissociation pressure of the alloy, respectively. As reference the measurement is performed under Ar of 0.10 MPa as well. The charge experiment is carried out up to the capacities of 20 mAh as full capacity of ß-$Ni(OH)_2$ electrode. The charge curves under H_2 and Ar have similar shape, suggesting that the same electrochemical reaction would proceed independent of the H_2 pressure in the cell.

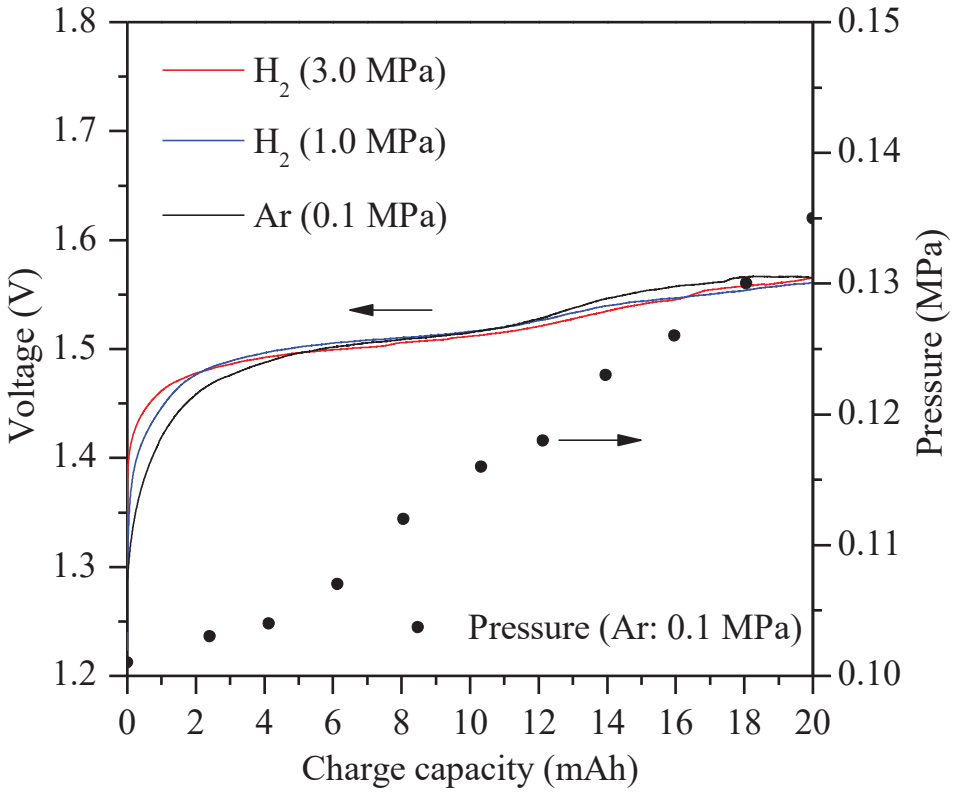

Fig. 4-3-3 Charge curves of HP-cell using $MmNi_{4.12}Co_{0.79}$ as a negative electrode material with current density of 2.54 $mAcm^{-2}$ (0.1 C) at 293 K, under several gas conditions.

Under Ar atmosphere of 0.10 MPa, gas pressure increases with the charging. Fig. 4-3-4 shows the gas chromatogram (GC) which is measured to analyze the released gas during the charging process under Ar. It is also shown GC of H_2 gas as reference. The released gas is assigned to H_2, and the partial pressure of H_2 in the HP-cell is increased from 0 to 0.035 MPa during the charge measurement.

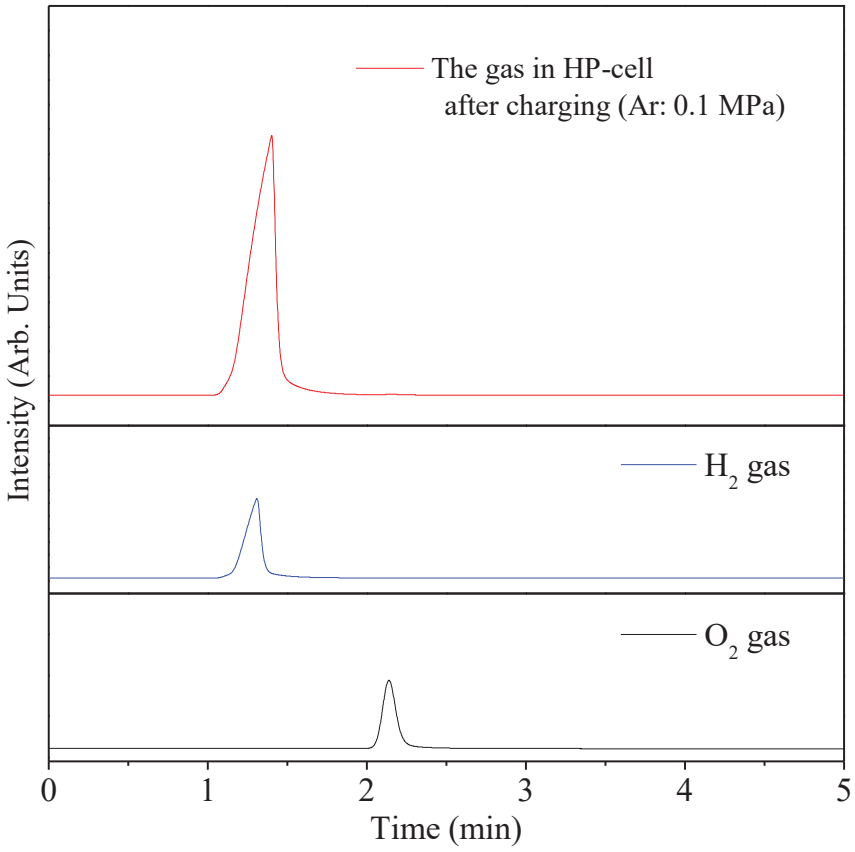

Fig. 4-3-4 Gas chromatogram (GC) of gas in the high-pressure electrochemical cell (HP-cell) during the charge measurement under Ar of 0.1 MPa (red), and GC of H_2 gas as reference sample.

The H_2 amount estimated from the pressure gain approximately corresponds to the formation of NiOOH from $Ni(OH)_2$ in the positive electrode. However, the molar ratio of $H/Ni(OH)_2$ is estimated to be 0.82. This molar ratio roughly corresponds to the

charge-discharge efficiency (87%) which is obtained from the charge/discharge capacity in Figure 4-3-1. However, it is presumed that the small amount of hydrogen (molar ratio: 0.18) is electrochemically absorbed in the alloy even if below the dissociation pressure, or electrochemically inactive $Ni(OH)_2$ remains.

"Fuel Cell/Battery (FCB)" which combined the Ni-MH battery and fuel cell system, has been proposed to realize high capacity energy storage [12]. At the FCB system, hydrogen and oxygen are released by over charge. At the Ni-MH/H_2 battery proposed in this work, only hydrogen is released by full charge and released gas is different from FCB system.

Fig. 4-3-5 shows discharge curves of the HP-cell composed of NiOOH electrode and the hydrogenated $MmNi_{4.12}Co_{0.79}$ electrode under different gas conditions. As described above, the discharge capacity of the cell under 3.0 MPa of H_2 is 17.4 mAh which is higher capacity than the theoretical capacity of MH. The discharge capacities are drastically decreased under 1.0 MPa of H_2 and 0.10 MPa of Ar, which is below the dissociation pressure. The small amount of discharge capacity under 1.0 MPa of H_2 suggests that the alloy absorbs small amount of hydrogen even if the metal hydride phase is unstable in this condition. However, when discharge measurement is carried out after refilling 3.0 MPa of H_2, the discharge capacity is extended to be higher capacity (14.3 mAh) than that under 0.1 MPa of Ar as shown Fig. 4-3-6. It is suggested that $MmNi_{4.12}Co_{0.79}$ is hydrogenated by refilling H_2 and the hydrogen is also utilized in the discharge process.

Noble metal catalysts such as Pt is required as catalysts for H_2 dissociation in the Ni-H_2 battery [13] [14]. On the other hand, the above results suggest that AB_5-type alloy plays a role as a hydrogen storage material and catalyst for H_2 dissociation at above the dissociation pressure in the proposed Ni-MH/H_2 battery. Thus, the high-cost catalysts are not necessary.

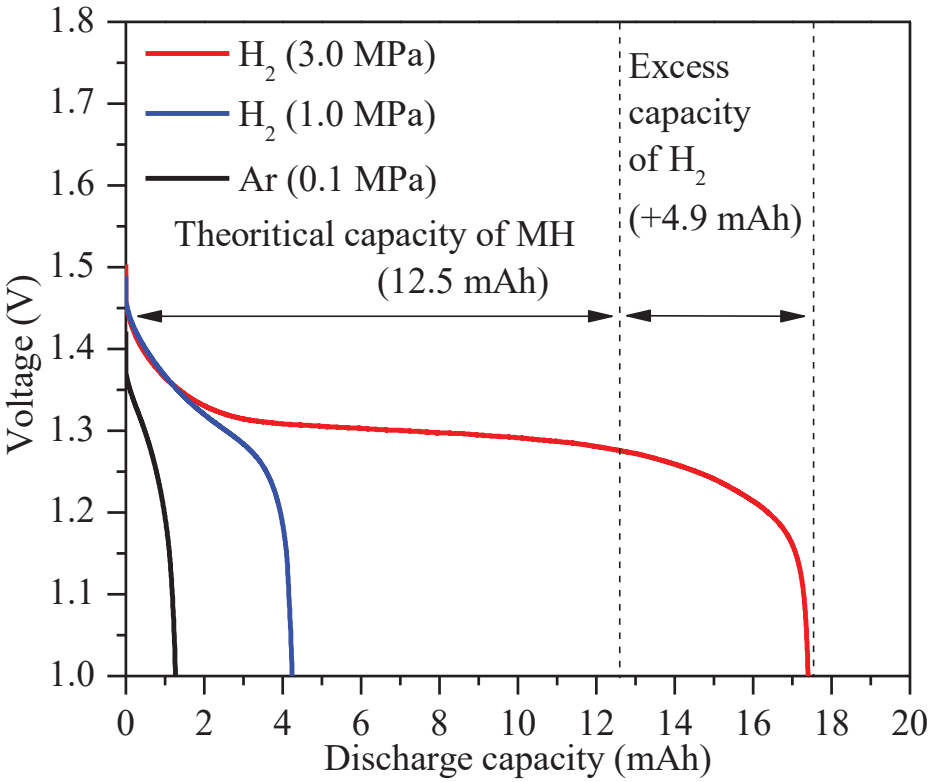

Fig. 4-3-5 Discharge curves of HP-cell using $MmNi_{4.12}Co_{0.79}$ as a negative electrode material with current density of 2.54 mA/cm^2 (0.1 C) at 293 K, under several gas conditions.

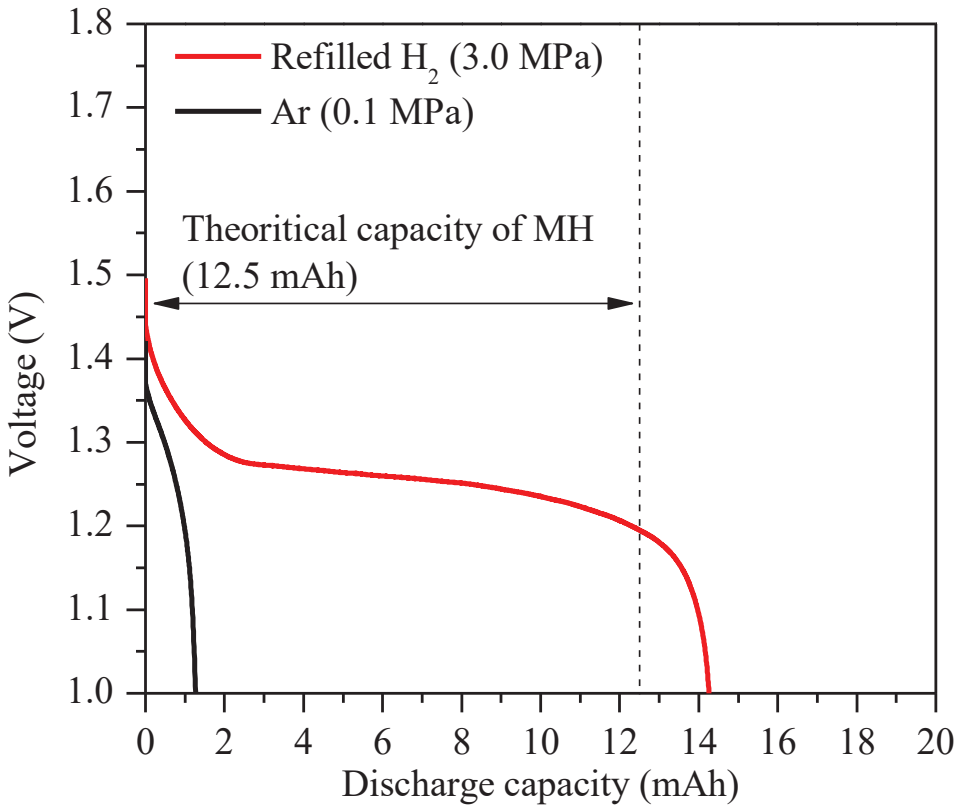

Fig. 4-3-6 Discharge curve of HP-cell using $MmNi_{4.12}Co_{0.79}$ as a negative electrode material with current density of 2.54 mA/cm^2 (0.1 C) at 293 K under (black) 0.1 MPa of Ar, and (red) discharge curve of this cell under refilled 3.0 MPa of H_2 after that.

4-4 Structural propeties of electrodes at charging/discharging

Fig. 4-4-1 shows XRD patterns of the positive electrodes after the charging and discharging processes. The peaks corresponding to Ni current corrector was observed for all samples as a background. XRD pattern of as-purchased positive electrode shows peaks at 2θ of 19.03, 33.09, 38.51, 59.07, and 62.67˚. These peaks originate in (001), (100), (101), (110), and (111) planes of ß-$Ni(OH)_2$ having $Cd(OH)_2$ type hexagonal structure [5]. The interlayer distance of ß-$Ni(OH)_2$ is 0.472 nm. After charging under 3.0 MPa of H_2 and 0.10 MPa of Ar, XRD patterns of positive electrode show peaks at 2θ of 18.97-18.95, 38.61, and 66.19-66.07˚. Those 3 peaks corresponds to diffraction from (001), (002), and (110) planes of β-NiOOH [15] [16]. The peaks at 19.03˚ of ß-$Ni(OH)_2$ shifts a little to lower angle of 18.97-18.95˚ after the charging, and then the interlayer distance of β-NiOOH is 0.474 nm. It is considered that the expansion of (001) plane of NiOOH is suppressed in the positive electrode by additives [16]. The peaks at 2θ of 12.81-12.83 and 25.81-25.67˚ originate in (003) and (006) planes of γ-NiOOH, respectively. The interlayer distance of γ-NiOOH is 0.694-0.695 nm. ß-$Ni(OH)_2$ was changed to β- and small amount of γ-NiOOH after the charging process under 3.0 MPa of H_2 and 0.1 MPa of Ar. The formation of γ structure can be explained by the overcharge [5]. Small amount of $Ni(OH)_2$ remained after the charging. After discharging, β- and γ-NiOOH is changed to ß-$Ni(OH)_2$ under H_2 of 3.0 MPa.

For the negative electrodes, the XRD patterns of negative electrode active materials after the charging and discharging processes are almost same because the AB_5-type metal hydride is unstable at atmospheric pressure and desorb H_2. (Fig. 4-4-2)

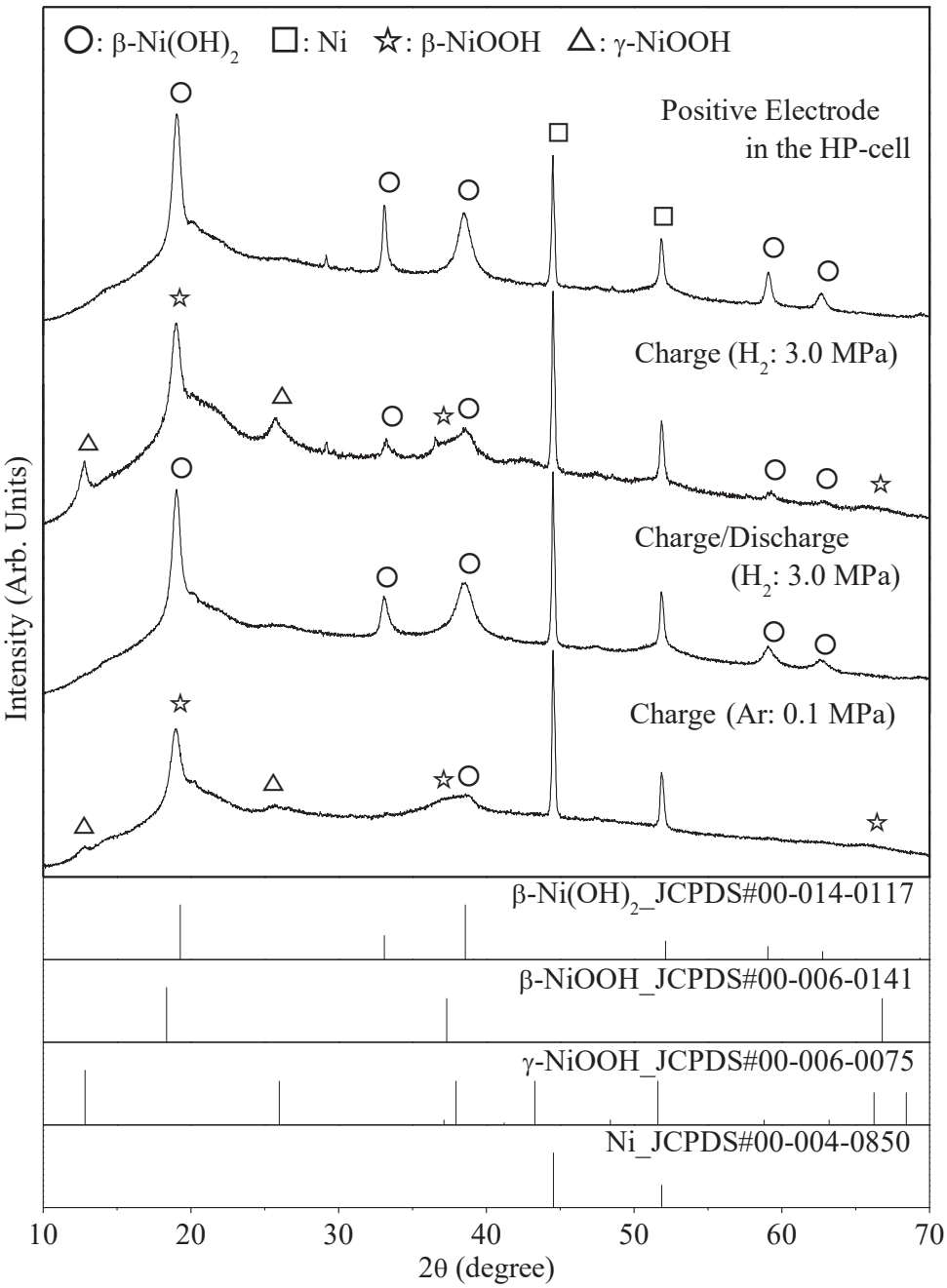

Fig. 4-4-1 XRD patterns of the positive electrodes as purchased and after charge/discharge conditions under H_2 and Ar gas together with the data of β-$Ni(OH)_2$ (JCPDS file No. 00-014-0117), β-NiOOH (JCPDS file No. 00-006-0141), γ-NiOOH (JCPDS file No. 00-006-0075), Ni (JCPDS file No. 00-004-0850).

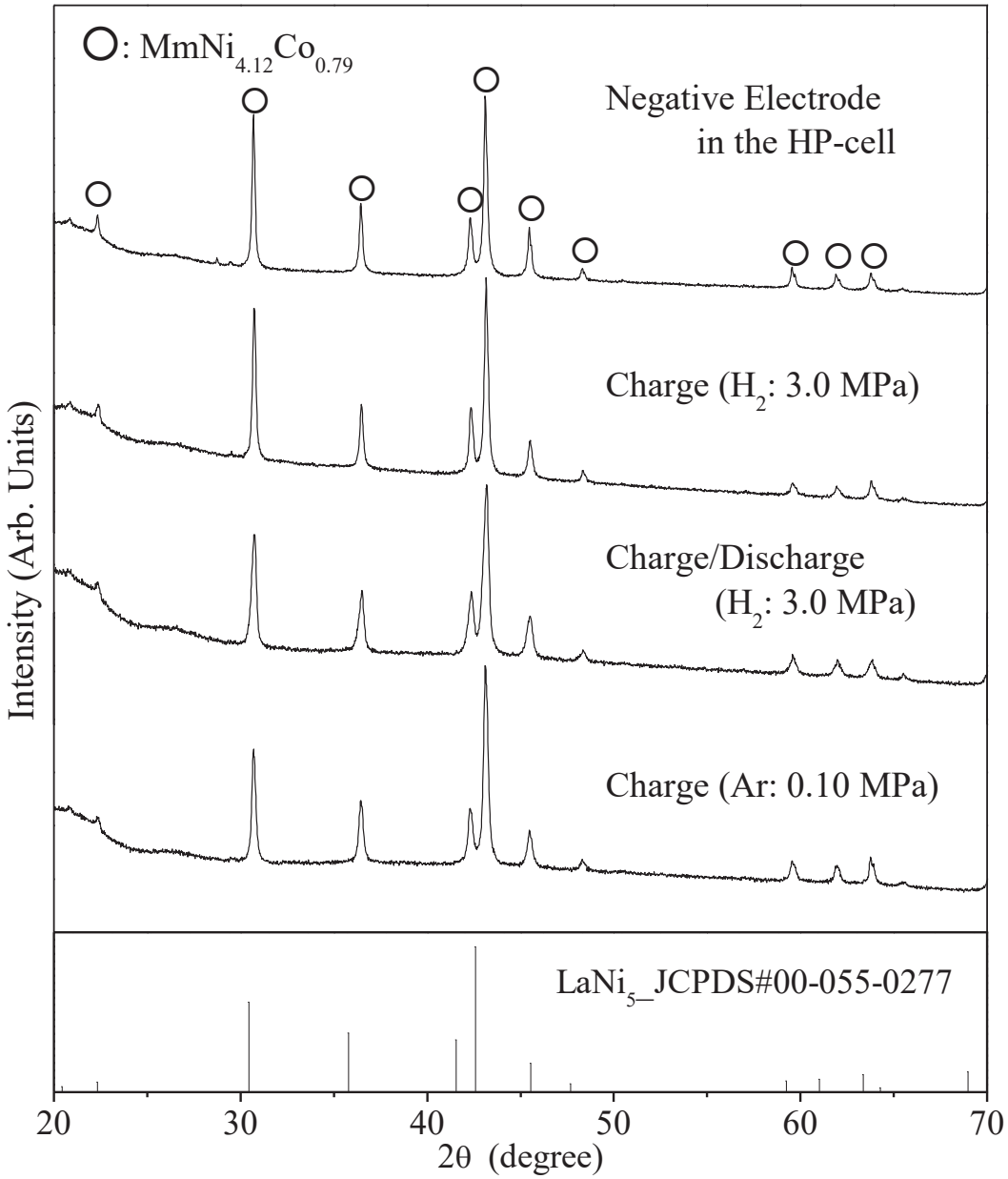

Fig. 4-3-7　XRD patterns of the negative electrodes as purchased and after charge/discharge conditions under H_2 and Ar gas together with the data of $LaNi_5$ (JCPDS file No. 00-055-0277).

4-5 Thermodynamic/Electrochemical analysis of metal hydrides

Thermodynamic parameters such as hydrogen dissociation pressure P of the hydrogen storage alloys are correlated with theoretical potential (E_{MH}) [11] [17]. The E_{MH} of these AB_5-type alloys are calculated by the following equation.

$$E_{\mathrm{MH}} = -0.828 - \frac{\mathrm{R}T}{2\mathrm{F}} \ln\left\{\frac{p_{\mathrm{eq}_{\mathrm{H_2}}}}{\mathrm{p}^0(T)}\right\} \tag{4-7}$$

where $p_{\mathrm{eq}_{\mathrm{H_2}}}$ is the dissociation pressure of hydrogen storage alloy (MPa), $\mathrm{p}^0(T)$ is standard pressure (0.101 MPa), R is gas constant (8.314 J $K^{-1}mol^{-1}$), T is temperature (K), F is Faraday constant (96485 $Cmol^{-1}$).

Standard electrode potential of hydrogen storage alloy is -0.828 V vs SHE (Standard Hydrogen Electrode: +0.000 V) [18]. The electromotive force of the cell (E_{EMF}) is determined by the theoretical potential difference of the electrodes using the hydrogen storage alloys and $Ni(OH)_2$ (+0.52 V vs SHE) [15] .

$$E_{\mathrm{EMF}} = 1.35 + \frac{\mathrm{R}T}{2\mathrm{F}} \ln\left\{\frac{p_{\mathrm{eq}_{\mathrm{H_2}}}}{\mathrm{p}^0(T)}\right\} \tag{4-8}$$

The average cell voltage which is assumed to be proportional to the E_{EMF} (open circuit voltage), was defined as the arithmetic mean of the charge and discharge voltages at 50% of each capacity. Fig. 5 shows the dependences of the average cell voltage on dissociation pressure of the negative electrode material at 293 K and 253 K. The E_{EMF} of the cell is also shown in the same Fig. 4-5-1 as a function of the dissociation pressure of AB_5-type alloy.

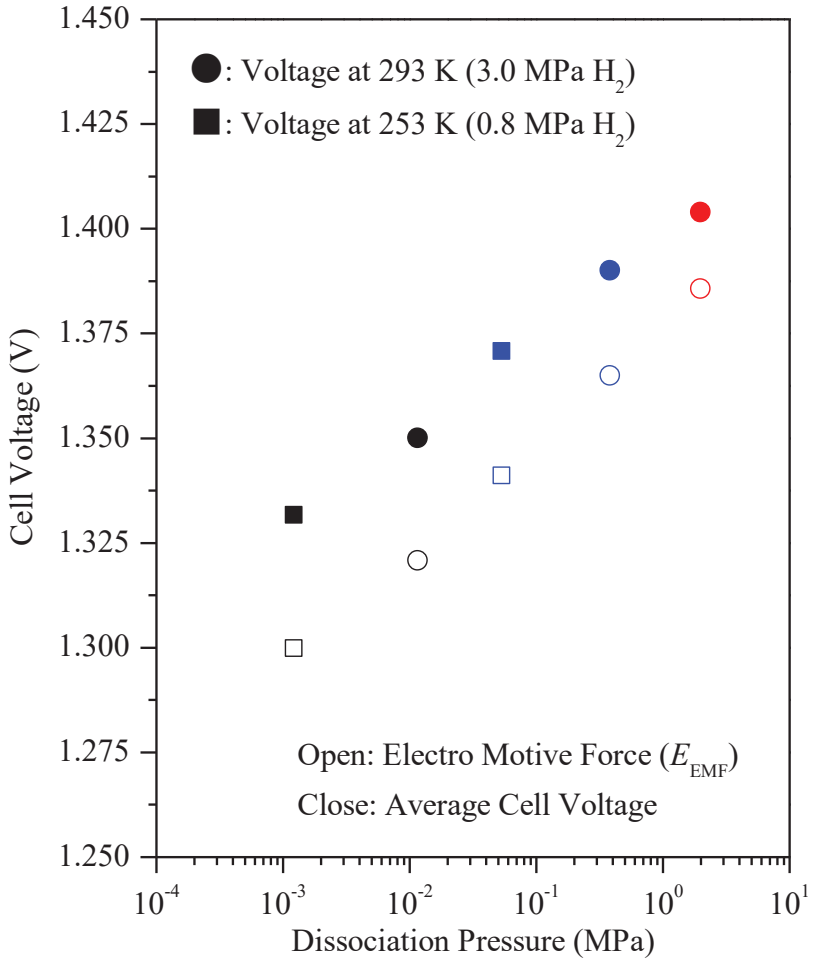

Fig. 4-5-1 The dependences of the average cell voltage and E_{EMF} on dissociation pressure of (red) $MmNi_{4.12}Co_{0.79}$, (blue) $MmNi_{4.16}Co_{0.6}Mn_{0.23}Al_{0.05}$, and (black) AB_5-type alloy in the commercial battery.

The experimental average cell voltages are determined by the thermodynamic parameters of H_2, whether the electrochemical reaction proceeds at the interface between the KOH aqueous solution and H_2 via the surface of AB_5-type alloy. However, Fig. 4-5-1 shows that the experimental average cell voltages linearly increase with the logarithm of the dissociation pressure. The slope is similar to the dependence of E_{EMF} on logarithm of dissociation pressure. This result suggests that the electrochemical reaction proceeds at the interface between the KOH aqueous solution and the AB_5-type alloy. The potential

of negative electrode can be approximately determined by thermodynamic parameters of AB_5-type alloy such as the dissociation pressure.

Additionally, the experimental average cell voltage was measured under several H_2 pressure. Fig. 4-5-2 shows the dependences of the average cell voltage on H_2 pressure. The experimental average cell voltages used $MmNi_{4\text{-}12}Co_{0.79}$ are approximately constant even at different internal pressures in the cell (Average: 1.41 V). In the case of using the commercial negative electrode, it is also indicated the similar trend exists (Average: 1.36 V).

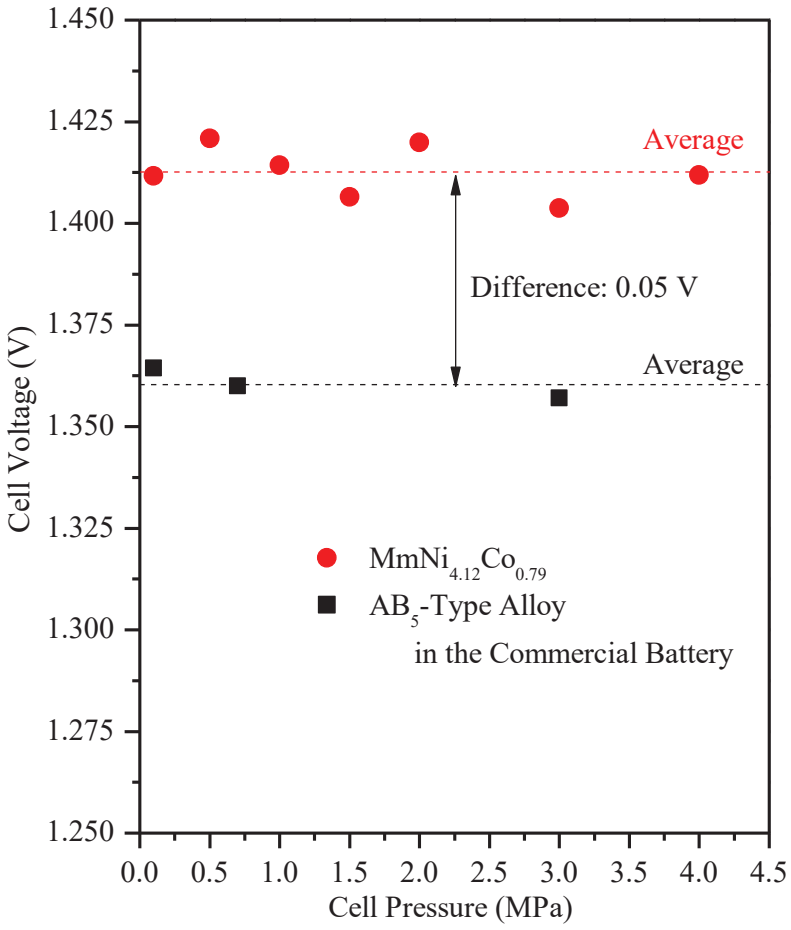

Fig. 4-5-2 The dependence of the cell voltage on H_2 pressure in the HP-cell using electrode of $MmNi_{4.12}Co_{0.79}$ and AB_5-type alloy in the commercial battery at 293 K

The difference in the average of the cell voltage by the negative electrode materials corresponds to the results in Fig. 4-5-2. It is indicated that the electrochemical reaction doesn't proceed at the interface between KOH aqueous solution and H_2. This result is different from Ni-H_2 battery using Pt-based catalyst [18].

The above results about experimental average voltage of the cell suggested that hydrogen gas is released after passing through the alloy in the form of atoms and the gas is dissociated into atoms and pass through the alloy during the charging and discharging processes, respectively. Therefore, at the later stage of charge and initial stage of discharge as shown Fig. 4-5-3, the overall reaction can be expressed by the following equation:

$$(1-x)\mathrm{Ni(OH)_2} + x\mathrm{MH} \leftrightarrow \frac{1-x}{2}\mathrm{H_2} + x\mathrm{MH} + (1-x)\mathrm{NiOOH} \qquad (4\text{-}9)$$

$$x\text{: } \frac{\text{Number of H atom in MH}}{\text{Number of H atom in MH and gas}}$$

where x is the ratio of the number of hydrogen atoms in MH to the total number of hydrogen atoms in MH and compressed hydrogen. x is in the regions of $0<x<1$. Hydrogen molecules dissociate into atoms and pass through MH during discharging.

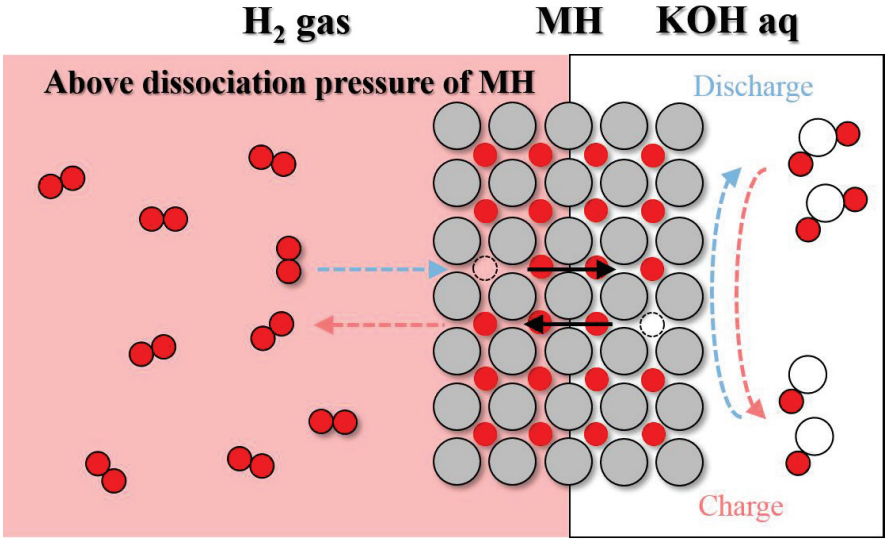

Fig. 4-5-3 Schematic diagram of the charge/discharge reaction mechanism on hybrid negative electrode using MH with high dissociation pressure and high-pressure H_2, at the later stage of charge and initial stage of discharge

At the initial stage of charge and at the later stage of discharge, the conventional reaction according to the equation below occurs as shown Fig. 4-5-4 [18]:

$$x\mathrm{Ni(OH)_2} + x\mathrm{M} \leftrightarrow x\mathrm{NiOOH} + \mathrm{xMH} \tag{4-10}$$

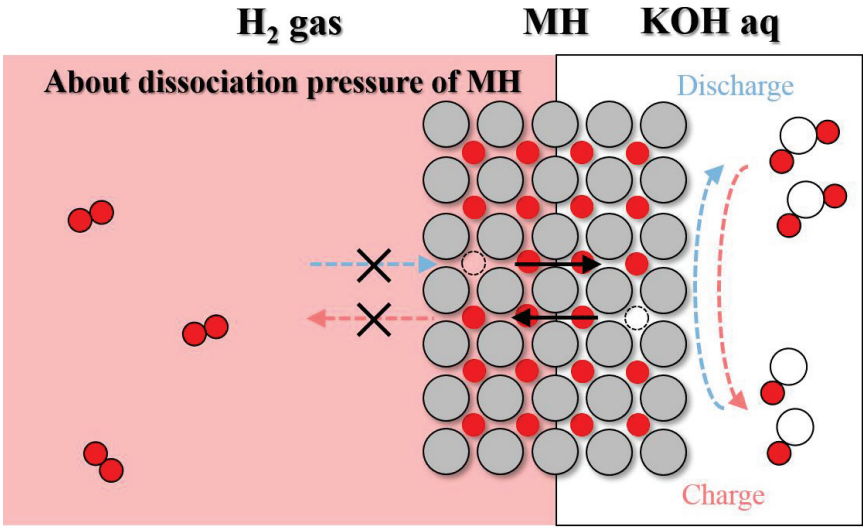

Fig. 4-5-4 Schematic diagram of the charge/discharge reaction mechanism on hybrid negative electrode using MH with high dissociation pressure and high-pressure H_2, At the initial stage of charge and at the later stage of discharge.

The total reaction is expressed by the following equation.

$$\mathrm{Ni(OH)_2} + \mathrm{M} \leftrightarrow \mathrm{NiOOH} + \frac{1-x}{2}\mathrm{H_2} + x\mathrm{MH} \quad (0 < x < 1) \tag{4-11}$$

The hydrogen-based energy storage system is composed of electrolyser, hydrogen storage tank, and fuel cell. The total efficiency is about 40%. The energy storage and generation efficiency of Ni-MH battery is 70-90% [19]. In this work, coulombic efficiency is 87-92% and energy efficiency is 74-76% (see Fig. 4-3-2). The energy efficiency is similar to Ni-MH battery [19] and two times larger than that of the hydrogen-based energy storage system. Therefore, "Hybrid Nickel-Metal Hydride/Hydrogen (Ni-

MH/H_2) Battery" provides high capacity and high efficiency hydrogen-based energy storage system reduced rare earth element.

Reference

[1] G. Sandrock, Journal of Alloys and Compounds, 293-295 (1999) 877-888.

[2] F. Cuevas, J.M. Joubert, Applied Physics A, 238 (2001) 225-238.

[3] E.W. Lemmon, M.O. McLinden, D.G. Friend, in: P.J. Linstrom, W.G. Mallard (Eds.) "Thermophysical Properties of Fluid Systems" in NIST Chemistry WebBook, NIST Standard Reference Database Number 69, National Institute of Standards and Technology, https://webbook.nist.gov/chemistry/, Gaithersburg, MD, 20899.

[4] W. Chen, G. Li, A. Pei, Y. Li, L. Liao, H. Wang, J. Wan, Z. Liang, G. Chen, H. Zhang, J. Wang, Y. Cui, Nature Energy, 3 (2018) 428-435.

[5] P. Oliva, J. Leonardi, J.F. Laurent, C. Delmas, J.J. Braconnier, M. Figlarz, F. Fievet, A.d. Guibert, Journal of Power Sources, 8 (1982) 229-255.

[6] M. Latroche, A. Percheron-Guégan, Y. Chabre, J. Bouet, J. Pannetier, E. Ressouche, Journal of Alloys and Compounds, 231 (1995) 537-545.

[7] T. Vogt, J.J. Reilly, J.R. Johnson, G.D. Adzic, J. McBreen, Journal of The Electrochemical Society, 146 (1999) 15-19.

[8] M.H. Mendelsohn, D.M. Gruen, A.E. Dwight, Nature, 269 (1977) 45-47.

[9] Y. Osumi, H. Suzuki, A. Kato, K. Oguro, S. Kawai, M. Kaneko, Journal of The Less-Common Metals, 89 (1983) 287-292.

[10] Y. Kojima, Y. Kawai, S.i. Towata, T. Matsunaga, T. Shinozawa, M. Kimbara, Journal of Alloys and Compounds, 419 (2006) 256-261.

[11] C.S. Wang, X.H. Wang, Y.Q. Lei, C.P. Chen, Q.D. Wang, International Journal of Hydrogen Energy, 22 (1997) 1117-1124.

[12] B. Choi, D. Panthi, M. Nakoji, T. Kabutomori, K. Tsutsumi, A. Tsutsumi, International Journal of Hydrogen Energy, 40 (2015) 6197-6206.

[13] J. Giner, Journal of The Electrochemical Society, 122 (1975) 4-4.

[14] L.H. Thaller, A.H. Zimmerman, in, 2003.

[15] S.U. Folk, Journal of The Electrochemical Society, 107 (1960) 661-667.

[16] M. Oshitani, T. Takayama, K. Takashima, S. Tsuji, Journal of Applied Electrochemistry, 16 (1986) 403-412.

[17] A. Jain, E. Kawasako, H. Miyaoka, T. Ma, S. Isobe, T. Ichikawa, Y. Kojima, Journal of Physical Chemistry C, 117 (2013) 5650-5657.

[18] D. Linden, T.B. Reddy, Handbook of Batteries. 3rd, 2002.

[19] W.H. Zhu, Y. Zhu, Z. Davis, B.J. Tatarchuk, Applied Energy, 106 (2013) 307-313.

5 Conclusion

In this thesis, we proposed and studied high capacity and high efficiency energy storage technique with new concept based on the technology of secondary battery and hydrogen.

We proposed “Hybrid Nickel-Metal Hydride/Hydrogen (Ni-MH/H_2) Battery” using AB_5-type metal hydride (MH) with high dissociation pressure (>0.1 MPa) and high-pressure hydrogen gas (H_2) as negative electrode materials. The basic properties and principle of this concept were discussed based on the experimental results. The reversible hydrogen capacities of the MH with high dissociation pressure were 1.4-1.5 wt.%, and theoretically calculated electrochemical capacity were 380-400 mAh/g. This capacity was higher than the value of the AB_5-type alloy in commercial battery (capacity: below 300 mAh/g, dissociation pressure: 0.011 MPa at 293 K). It was expected that gravimetric/volumetric energy densities of this battery could be controlled by the ratio of MH and hydrogen amounts. The calculated gravimetric energy density of this hybrid battery increased up to 1.5 times of the conventional Ni-MH battery with low content of rare-earth element which is 32 wt.% of the Ni-MH battery.

The electrochemical properties of this concept under high-pressure H_2 atmosphere were investigated by the specially designed high-pressure electrochemical cell. It was confirmed that hydrogen gas was reversibly utilized for charge and discharge reactions at the above dissociation pressure of the AB_5-type alloy. It is experimentally demonstrated that a concept of the hybrid battery can be realized. The energy efficiency of this cell was 74-76%, which is the similar efficiency to that of commercial Ni-MH battery. This efficiency was also about two times of the hydrogen energy system composed of water electrolyser, hydrogen storage tank, and fuel cell (about 40%). The cell voltage which is an averaged value of charge and discharge voltages at 50% of the capacities was consistent with the theoretical voltage estimated by dissociation pressure of the AB_5-type alloys. This indicates that the both of hydrogen sorption and electrochemical reactions proceed via the hydrogen absorption state in the form of atoms, in other words, H_2 gas is dissociated into atoms and pass through the alloy during the charging and discharging processes, respectively while the cell voltage was

constant in despite of the internal pressure variation. It was considered that MH does not act catalytic role like Pt.

Acknowledgments

I would like to express my sincere gratitude to my supervisor Prof. Yoshitsugu Kojima throughout the course of this work. I appreciate that he gave me much advise and support on research activities such as direction and discussion of research. Prof. Takayuki Ichikawa also gave me various advises and support in spending my doctoral course. I am deeply grateful to him for giving opportunities such as collaborative research and conference presentation. I would also like to express my thanks to especially Associate Prof. Hiroki Miyaoka for giving a lot of advice on experiments and preparing article. I appreciate that he gave me much time for discussion on detail.

I am sincerely grateful to Prof. Takashi Suzuki and Prof. Takahiro Onimaru who is my sub examiner of my doctoral thesis examination. They gave me significant suggestions and discussion on thesis.

I would like to my gratitude to Assistant Prof. Tessui Nakagawa who was supervisor of my master's course, for introducing this laboratory. I would also like to express my appreciation to Associate Prof. Ryota Kondo from Kansai University, who gave me valuable advice and experimental opportunities. I am also grateful to Dr. Abdelouahab El Kharbachi for giving opportunity to collaborated research.

I would like to my sincere thanks all people who involved throughout the spent time in this laboratory. I am especially grateful to Mr. Keita Nakajima and Mr. Kenta Shinzato who spent a long time together. I would also like to thank Mr. Takashi Komoto who had advanced related researches. I also thank Mr. Ryo Ohata to live together. I would also like to especially appreciate Associate Prof. Ankur Jain, Ms. Misao Mukoda, Ms. Saori Inagaki, and Mr. Tomoyuki Ichikawa for supporting in this laboratory.

Finally, I would like to express my gratitude to my family and friends for supporting my advance of doctoral course.

公表論文

(1) Hybrid nickel-metal hydride/hydrogen battery
Hiroki Uesato, Hiroki Miyaoka, Takayuki Ichikawa, and Yoshitsugu Kojima
International Journal of Hydrogen Energy, **44(8)**, 4263-4270 (2019).

参考論文

(1) MgH_2-CoO: A conversion-type composite electrode for $LiBH_4$-based all-solid-state lithium ion batteries
Abdelouahab El Kharbachi, Hiroki Uesato, Hironori Kawai, Sigurd Wenner, Hiroki Miyaoka, Magnus H. Sørby, Helmer Fjellvåg, Takayuki Ichikawa, and Bjørn C. Hauback
RSC Advances, **8(41)**, 23468-23474 (2018).